batteries

MDPI

Review

A Review of Nail Penetration and Thermal Abuse Tests of Lithium-Ion Batteries and Their Emission Characterization

Ananthu Shibu Nair [1], Xiao-Yu Wu [1,*], Prodip K. Das [2,*] and Michael Fowler [3,*]

[1] Department of Mechanical and Mechatronics Engineering, University of Waterloo, 200 University Avenue West, Waterloo, ON N2L 3G1, Canada; ashibuna@uwaterloo.ca
[2] School of Engineering, University of Edinburgh, Edinburgh EH9 3FB, UK
[3] Department of Chemical Engineering, University of Waterloo, 200 University Avenue West, Waterloo, ON N2L 3G1, Canada
* Correspondence: xiaoyu.wu@uwaterloo.ca (X.-Y.W.); prodip.das@ed.ac.uk (P.K.D.); mfowler@uwaterloo.ca (M.F.)

Abstract

Lithium-ion batteries (LIBs) are pivotal in electric vehicles (EVs), grid storage, and portable electronics, but their high energy density introduces safety risks, particularly thermal runaway (TR). TR can lead to fires, explosions, and hazardous emissions, posing severe health and environmental threats. Experimental investigation of TR commonly relies on abuse testing methods, among which mechanical abuse via nail penetration (NP) and thermal abuse (TA) are widely used to simulate crash-induced and heat-driven failure scenarios, respectively. This review provides a comprehensive and comparative synthesis of NP and TA testing methodologies, examining how variations in test configuration, cell parameters (capacity, state of charge, and chemistry), and environmental conditions influence TR behavior and emission characteristics. Particular emphasis is placed on comparing reported emission profiles from NP- and TA-triggered TR events, including CO_2, CO, HF, hydrocarbons, and solvent vapors, and identifying the methodological origins of discrepancies across studies. By systematically linking emission variability to gas collection methods, analytical techniques, and data normalization approaches, this review highlights key limitations in current testing standards related to emission characterization. Finally, recommendations are offered for harmonizing abuse testing protocols and improving experimental design to enhance reproducibility, enabling meaningful cross-study comparison, and supporting safer deployment of LIBs in high-risk applications such as EVs and grid-scale energy storage.

Keywords: lithium-ion batteries; nail penetration tests; thermal abuse tests; emissions; thermal runaway

Check for updates

Academic Editor: Matthieu Dubarry

Received: 6 January 2026
Revised: 6 February 2026
Accepted: 13 February 2026
Published: 18 February 2026

Copyright: © 2026 by the authors. Licensee MDPI, Basel, Switzerland. This article is an open access article distributed under the terms and conditions of the Creative Commons Attribution (CC BY) license.

1. Introduction

The transport sector emits significant amounts of greenhouse gases. For example, in 2023, the transport sector accounted for 23% of Canada's total GHG emissions, which was one percentage point higher than the previous year [1]. Globally, transport remains a major contributor to GHG emissions: in 2024, the transport sector emitted about 8.4 Gt $CO_{2\text{-equivalent}}$, representing roughly 15.9% of total global GHG emissions [2]. Therefore, the past decade has seen a significant rise in the global effort to transition towards cleaner energy systems within the transport sector [3–6]. For example, Transport Canada has set a goal of achieving net-zero emissions by 2050, which is highlighted in the 2030 Emissions

Reduction Plan. The Canadian government also has a mandate that requires 100% zero-emission light-duty vehicle sales by 2035 [7]. Globally, many other countries and regions have set similar deadlines. The International Energy Agency (IEA) notes that in its "net-zero" scenario, light-duty vehicle sales worldwide, including cars and vans, are projected to become fully zero-emission by 2035 [8]. These global efforts have led to a rapid expansion of electric vehicles (EVs) within the transportation sector [9]. For instance, in 2023, Canada's zero emission vehicle (ZEV) market share reached 11.7%, a significant increase from 3.1% in 2019. The ZEVs, encompassing both battery electric vehicles (BEVs) and plug-in hybrid electric vehicles, saw sales exceeding 15% by the third quarter of 2024 in Canada [10]. By the second quarter of 2024, the adoption rate of BEVs alone in Canada hit 12.2% [11].

Among all the rechargeable batteries, lithium-ion batteries (LIBs) are favored in EVs for their high energy density and extended shelf life [12,13]. Compared to lead-acid or nickel-metal hydride batteries, LIBs have a higher cathode potential, and hence, higher energy density, and they also have greater cycle life, as shown in Figure 1 [14]. Moreover, LIBs possess a high power-to-weight ratio, improved thermal stability, and a low self-discharge rate [15–18].

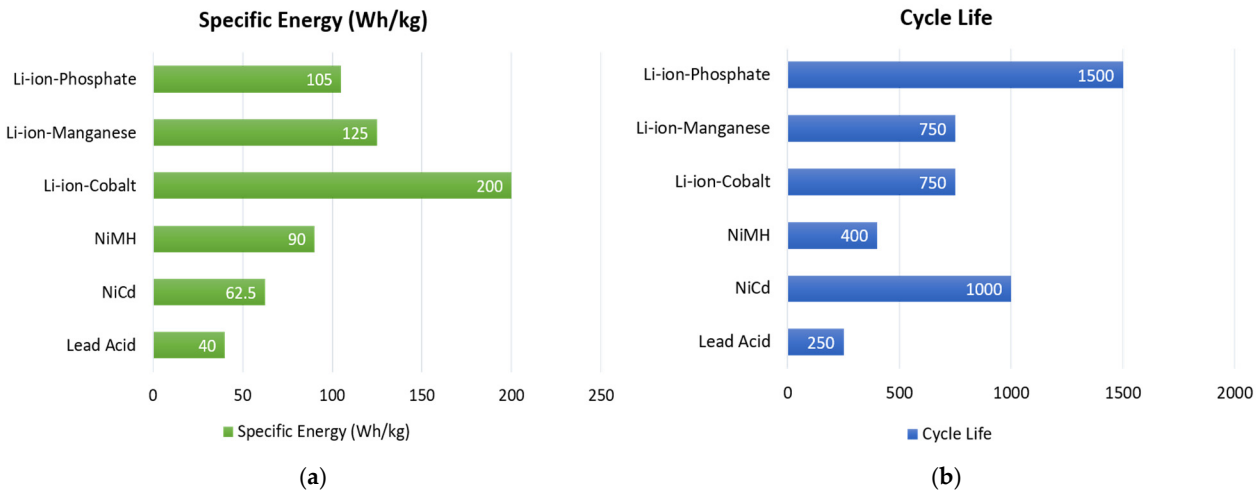

Figure 1. Specific energy (**a**) and cycle life (**b**) comparison between LIBs and other secondary cells. Recreated originally from [14].

As a result, LIB demand has risen, and its use has become widespread. For example, in 2023, the sales of EVs accounted for 95% of the increase in global LIB demand, totaling over 750 Gigawatt-hours [19]. China dominated EV LIB manufacturing, while the United States and Europe experienced the most rapid market development [20]. Besides EVs, LIBs have seen widespread adoption in consumer electronics ranging from cellphones to power tools. Furthermore, LIBs also play a vital role in grid energy storage systems, as battery energy storage systems (BESSs) contribute to reliable energy supplies from storage grids and increase the economic viability of renewable energy sources. Currently, LIBs represent more than 90% of the global grid battery storage market [21].

The widespread use of LIBs and their high energy density introduces safety risks associated with thermal runaway (TR), which can result in fires, explosions, and hazardous emissions [22]. Hence, it requires significant effort to study TR carefully to understand its mechanisms and potential impacts and to develop strategies to avoid TR (the underlying mechanisms of TR will be discussed in detail in later Section 3). The goal of this review article is to summarize the latest developments in using two major abuse testing methodologies, i.e., mechanical abuse via NP and TA, to study the TR of LIBs. We review test configurations, cell parameters (e.g., capacity, state-of-charge, chemistry), and environmen-

tal conditions that can influence TR results. In addition, emission profiles from the resulting TR, including CO_2, CO, HF, hydrocarbons, and other solvent vapors are also summarized and examined to understand their toxicity and environmental impact.

While prior reviews primarily address thermal runaway mechanisms, safety standards, or abuse testing methods, emissions are often discussed only qualitatively or in isolation. In contrast, this work systematically compares reported emission species and magnitudes from NP- and TA-induced thermal runaway and links observed discrepancies to test configuration, environment, gas collection methods, analytical techniques, and data normalization. By consolidating emission data across different chemistries, cell formats, and states of charge, the review highlights key gaps in current testing practices and provides practical recommendations for improving reproducibility and cross-study comparability.

1.1. LIB Basics

This section provides a high-level summary of basic information about LIBs to set up a foundation for later discussions on TR tests. Readers are encouraged to refer to other in-depth review articles to gain a full understanding of LIBs. A comprehensive overview of LIB technology is provided by Sharma et al., who review the fundamental electrochemical principles, cell architecture, and major performance limitations of LIBs [23]. Focusing on battery materials, Khalid et al. present an in-depth review of recent progress in cathode and anode development; their study compares various material chemistries in terms of energy density, cycle life, and thermal stability, providing valuable insight into how material selection influences overall battery performance [24]. Safety-focused aspects of LIBs are thoroughly reviewed by Yao et al., who examine failure mechanisms such as TR, gas generation, and internal short-circuiting [25]. Zanoletti et al. focus on battery recycling and sustainability, evaluating current technologies and proposing strategies to improve recovery efficiency [26]. In terms of modelling and advanced management systems, Madani et al. review the techniques, challenges and future perspectives, covering SOC estimation, health monitoring, and emerging machine-learning approaches [27].

1.1.1. Internal Structure and Form Factors

LIBs were first introduced commercially by Sony Corporation in 1991 [28]. Since then, significant advancements have enhanced their energy capacity, safety, and performance by improving cell materials, structures, shapes, and sizes. Currently, LIB cells are produced in varying form factors, namely coin, cylindrical, pouch, and prismatic, to adapt to specific application requirements.

A LIB cell typically consists of two electrodes, i.e., an anode and a cathode, separated by a polymer-based separator and submerged in an electrolyte solution that is held together by the binder. In a coin cell, the electrodes and separator are arranged in singular flat layers, whereas in a cylindrical or pouch cell, multiple layers are rolled into a jelly-roll configuration [29–31]. The electrolyte, consisting of lithium salts, organic solvents, and various additives, facilitates the transfer of lithium ions between the electrodes during charge and discharge cycles, while enhancing thermal stability [32].

1.1.2. Charging and Discharging Mechanisms

During a charge cycle, lithium ions migrate from the positive electrode (cathode) to the negative electrode (anode). The anode, typically composed of graphite, accommodates these ions through intercalation, where the lithium ions are stored between the graphite layers. During discharge, the process reverses and the lithium ions move back to the cathode, while electrons flow through the external circuit, providing power to the connected device [33–35]. The separator, a porous polymer membrane between the electrodes, plays a

critical role by allowing lithium ions to pass freely between the electrodes during charge-discharge cycles, while preventing direct contact between them [36].

1.1.3. Cathode Materials and Performance Impact

The cathode material plays a major role in determining the overall properties of an LIB cell. It largely governs the cell voltage, which in turn influences the energy capacity, regardless of the anode material [37,38]. They are often made of oxides of metals such as nickel, manganese, cobalt, iron, and aluminum, and the cathode chemistry impacts battery safety, charge transfer, and cell capacity [39]. Some of the common cathode materials include lithium-nickel manganese cobalt oxide (NMC), lithium ferro phosphate (LFP), lithium manganese oxide (LMO), and lithium-nickel cobalt aluminum oxide (NCA or LCO) [40,41].

1.2. LIB Safety Incidents

1.2.1. Global Rise in Battery Incidents

Concurrently with the expansion of the battery industry, there has also been an increase in safety incidents, prompting heightened attention from both consumers and manufacturers [42–44]. Figure 2a illustrates the rising number of LIB safety incidents reported across 12 countries including Canada, China, Germany, India, Japan, the Netherlands, Norway, Singapore, South Korea, Sweden, the United States, and the United Kingdom, between 2016 and 2024. Similarly, a clear upward trend in the incidents over time is also observed in Canada, as shown in Figure 2b. While TR is a mechanistic phenomenon at the cell-level, real-world battery incidents often represent system-level outcomes where TR initiation, propagation, and environmental conditions jointly determine the severity of fires, explosions, and hazardous emissions.

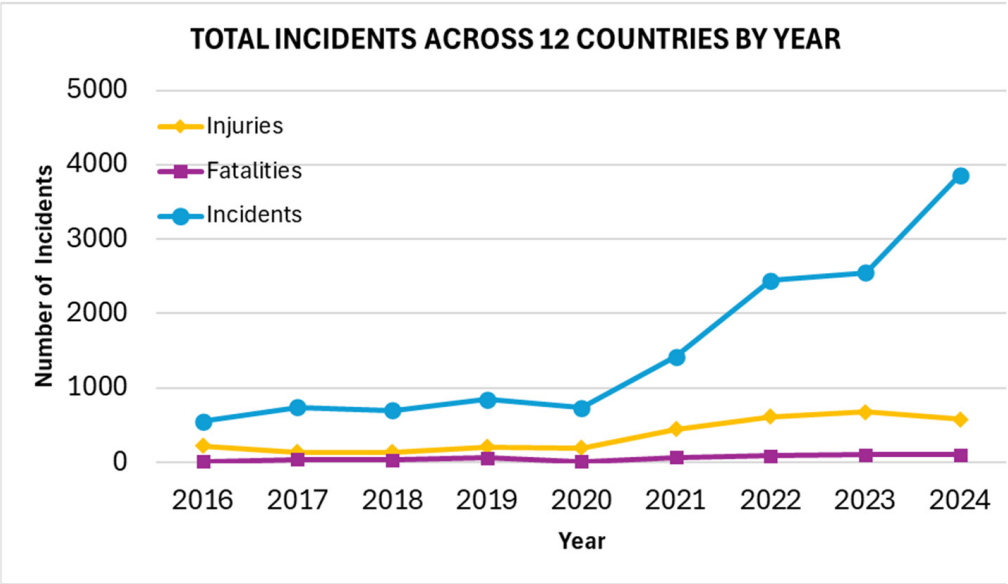

(**a**)

Figure 2. *Cont.*

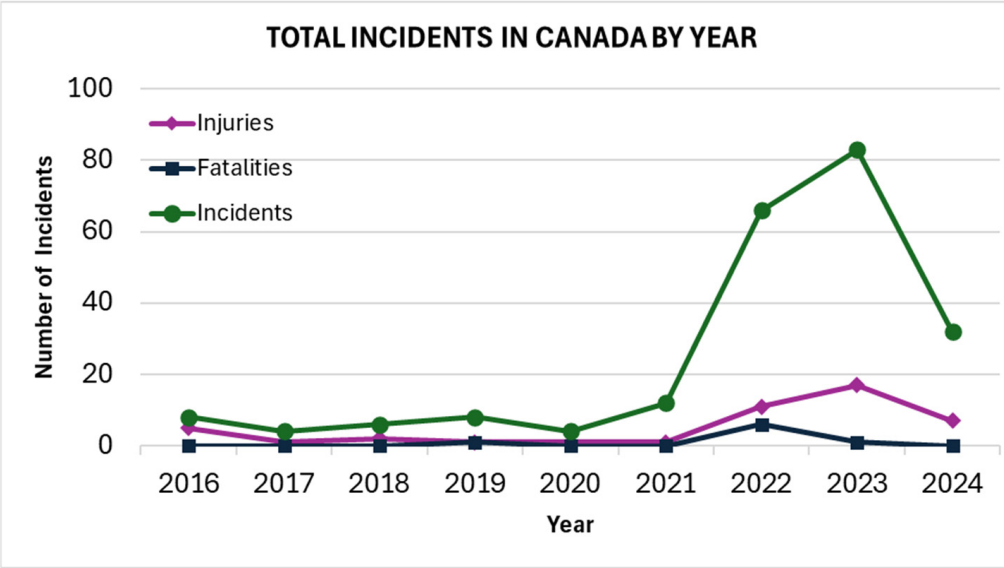

(**b**)

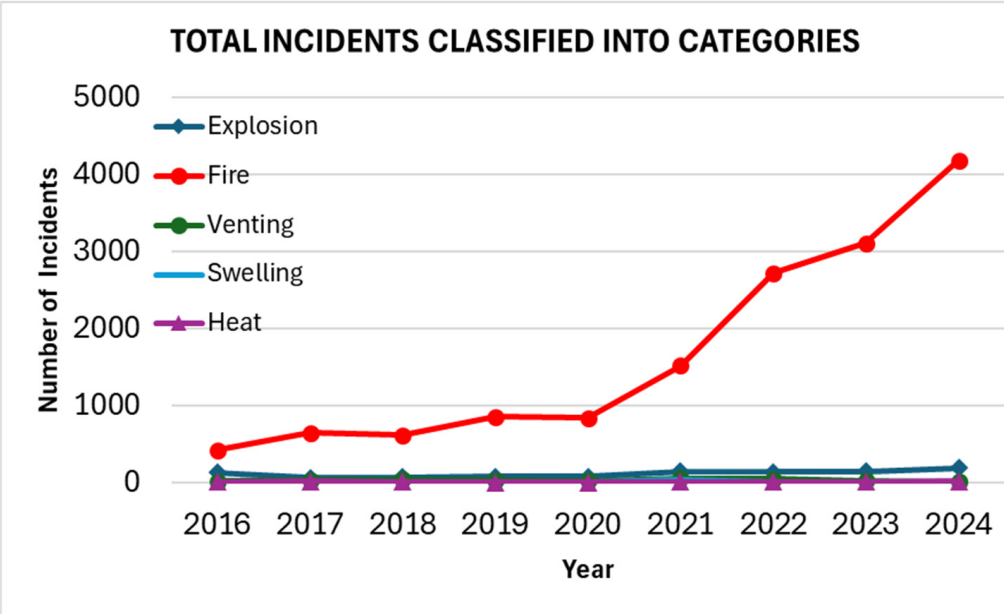

(**c**)

Figure 2. (**a**) Increase in incidents related to LIBs, e.g., injuries, fatalities, and incidents, in 12 countries between 2016 and 2024, (**b**) increase in incidents related to LIBs, e.g., injuries, fatalities, and incidents, in Canada between 2016 and 2024, (**c**) LIB incidents from 12 countries between 2016 and 2024 are classified based on battery status, e.g., explosion, fire, venting and heat. Recreated originally from [45].

1.2.2. Health and Environmental Hazards

Safety incidents involving EV batteries (e.g., LIBs) typically result in fires as shown in Figure 2c, which can cause catastrophic passenger injuries and substantial reputational damage to battery manufacturers, ultimately hindering the wider adoption of emerging technologies. Moreover, incidents involving explosions, venting, and fires, along with the release of toxic emissions present significant hazards to human health and environmental safety [46], which are disastrous for the surrounding environment and affected individuals [45]. For example, HF (hydrofluoric acid) is one of the dangerous emission com-

ponents that can cause eye irritation, skin burns, and respiratory diseases under prolonged exposure [18].

1.2.3. Notable Incidents in North America

Recent years have seen a few significant LIB incidents in North America. The City of Toronto recorded a 162% increase in LIB fires between 2022 and 2024 [47]. The City of Vancouver reported LIB fires as one of the leading contributors to urban fire incidents [48]. In September 2024, a fire involving LIBs on a ship in Montréal port released large volumes of HF gas and particulate matter (PM) into the atmosphere, severely polluting the environment and jeopardizing the health and safety of both firefighters and surrounding communities [49]. In the USA, reports from the first quarter of 2024 revealed a rising number of LIB fire incidents in New York City, where there were 267 LIB fires in 2023, leading to 150 injuries and 18 deaths [50].

1.2.4. Firefighting Challenges

As seen in Figure 2c, fires are the most common outcome associated with LIB failure. Firefighters reported that extinguishing an EV fire caused by LIBs can require up to 3 h and 40 times more water compared to extinguishing a fire produced from an internal combustion engine that could be extinguished in only about 20 min [51,52]. This presents significant challenges for firefighting, necessitating specialized equipment and training. However, a nationwide survey conducted in 2022 involving over 1000 USA first responders revealed that more than 40% of them received no safety training related to EV fires [53].

On the other hand, the hazards associated with LIB fires and their impact on human health are still unclear [54]. For example, to improve the understanding of the required decontamination procedures to ensure the safety of personal protective equipment (PPE), the Fire Protection Research Foundation (FPRF) of the US National Fire Protection Association is currently conducting studies on LIB fires and the associated health risks on firefighter exposure [55].

2. Regulatory and Testing Frameworks

2.1. Overview of LIB Safety Regulations

Due to potential safety hazards, global and regional regulations have been implemented for the transportation, storage, and testing of LIBs. Transportation and storage of LIBs are governed by well-established regulations and standards internationally. However, there is a lack of comprehensive compliance when it comes to safety testing. Only a few standards, such as SAE J2464, specify basic mechanical abuse test conditions, including those for nail penetration (NP) tests. These regulations are relatively recent and would benefit from more comprehensive and well-defined protocols, particularly regulations addressing the emissions generated during LIB failures.

2.2. UN-Level Transport and Storage Regulations

For transportation and storage of LIBs, the UN Manual of Tests and Criteria classifies LIBs under UN 3480 when shipped as standalone batteries, and under UN 3481 when packed with, or contained in equipment. The Manual also includes special provisions for LIB shipping. According to Provision 34, the regulations under UN 3480 and UN 3481 do not apply to domestic transportation of LIBs, provided that they are clearly marked with their watt-hour rating on the cell casing. Provision 123 exempts batteries from the requirements of the Manual if the total number of cells is fewer than 100, as these would be considered to be within a pilot or prototyping phase. Provision 137 applies to de-

fective batteries, while Provisions 138 and 157 apply to battery recycling, disposal, and labelling [56,57].

2.3. UN Manual Testing Requirements and Gaps

The UN Manual of Tests and Criteria (UN 38.3) also outlines several mandatory tests on representative LIB samples before transportation. These include altitude simulation, thermal cycling, vibration, shock, external short circuit, impact, overcharge, and forced discharge [58]. However, the impact tests are primarily intended to evaluate the mechanical integrity of the battery casing, rather than internal cell components. NP tests, which will be discussed later in Section 4 of this paper, are not included in the current UN Manual, representing a gap in standardized testing for certain safety-critical failure modes. While the manual addresses some of the important hazards as highlighted above, they do not fully capture TA scenarios such as overheating, or exposure to external fires. These phenomena are discussed in detail in Section 5, which focuses on the mechanisms and experimental study of TA in LIBs.

2.4. National Level Rules: Case Study from Canada

National regulations on LIB shipping and storage provide supplementary guidelines and requirements beyond those in the UN Manual. For example, Canada established several rules and regulations for the transportation and storage of LIBs, which are classified as dangerous goods and are subject to the Transportation of Dangerous Goods Act 1992 [59,60]. This act incorporates several conditions for LIB transport and shipment, supplementing the UN Manual by specifically addressing lithium metal and LIBs [61,62]. In addition to the UN requirements, the Act introduces further provisions, such as the mandatory inclusion of a safety-venting device to prevent explosions and adequate protection against external short circuits. However, the Act does not specify any design requirements for the overall safety system, nor does it address the need for preventing internal short circuits, which can be equally hazardous [63].

2.5. International Testing Standards and Methods

A variety of international testing standards were adopted in North America, including CSA C22.2 NO. 62133-2:20, UL 2580, UL 1642, UL 2054, IEC 62133 and SAE J2464. UL 2054 applies to household and commercial batteries, while UL 2580 is meant for batteries used in EVs [64,65]. IEC 62133 standard applies to different battery types including LIBs and outlines the safety requirements for batteries used in mobile applications. It highlights the safety requirements for portable batteries used in consumer electronics, including cellphones and laptops [66]. UL 2580, SAE J2464, and SAE J2929 apply to batteries used in electric and hybrid vehicles.

Some of these regulations assess safety risks by setting constraints on acceptable test outcomes. They are developed based on the battery type, application, and cell configuration. For example, UL 1642 is a safety standard for LIBs used in user-replaceable applications and includes 10 tests, such as crush and impact testing [64]. In addition, SAE J2929, a predecessor of SAE J2464, includes drop tests, TA, short circuit, etc., but does not contain requirements for NP tests.

Major LIB safety standards, e.g., GB/T 31485, IEC 62133, UL 2580, SAE J2464, VW PV8450, and USABC–GM, address abuse scenarios including heating, external short circuit, overcharge, overdischarge, and, in most cases, NP. TA protocols vary between fixed-temperature holds and controlled heating ramps, reflecting differences in targeted applications from portable electronics to electric vehicles. Short-circuit tests primarily differ in the applied resistance and termination criteria, ranging from limited-current conditions

to sustained hard shorts until fire, explosion, or thermal stabilization occurs. Chen et al. provided a detailed comparison among these standards [67].

Overcharge and overdischarge requirements show significant variability across standards, with some defining limits based on multiples of SOC and others using voltage thresholds, time limits, or venting as termination criteria. This results in markedly different stress severities even for nominally similar test categories [67].

NP testing is included in most EV-focused standards but is absent from IEC 62133, which primarily targets consumer electronics. Where specified, NP procedures in these standards differ substantially in penetration speed, nail diameter, and depth, ranging from slow, shallow penetration intended for early failure detection to full-depth, high-speed penetration designed to induce worst-case internal short circuits [67].

Overall, UL 2580 and SAE J2464 impose more severe and comprehensive abuse conditions suitable for automotive applications, while IEC 62133 adopts comparatively conservative requirements. The heterogeneity across standards highlights a lack of harmonization in abuse-test severity and methodology, particularly for mechanical abuse and emission-relevant failure modes.

2.6. SAE J2464: A LIB Abuse Testing Standard

SAE J2464 is a more recent standard that provides a detailed overview of safety and abuse testing procedures for LIBs at the cell, module, and pack-levels. These include NP, crush, thermal, and electrical abuse test methods [68]. The standard includes several TA tests including tests for thermal stability, cycling without thermal management, thermal shock cycling, high-temperature hazard, and single cell failure propagation resistance [69].

For NP, a steel nail with a 3 mm diameter is used for cells, and a 20 mm diameter nail is used for modules and packs, with a penetration speed of 8 cm/s. For crush tests, the required speed is $\leq$6 mm/min, much lower than that for NP. Crush tests must be conducted using a semicircular-ended rod, and the system must remain in the end condition for a certain period to observe whether additional reactions occur after deformation. The test termination conditions for crush may vary, including a one-third drop in cell voltage, deformation exceeding 15% of the cell, or the applied force reaching 1000 times the cell's weight [70].

3. Thermal Runaway in LIBs: Causes, Consequences, and Test Methodologies

3.1. What Is Thermal Runaway?

Safety incidents involving LIBs typically occur when the batteries enter thermal runaway (TR), which is a rapid uncontrollable heat-generating process driven by exothermic reactions. LIB modules are designed to operate within a specific temperature range and are typically equipped with battery management systems (BMS) to regulate heat dissipation through convection and ventilation. The optimal operating range of LIBs is typically between 15 and 35 °C and the recommended charging window is between 10 and 40 °C [71,72]. However, when the internal or external heat generation surpasses the dissipation capacity, the BMS loses its ability to regulate the temperature rise.

The exothermic heat generation ignites the flammable electrolytes and results in high-speed fire ejecta through the cell vent. Gupta et al. [73] classify the propagation of this fiery ejecta into three ignition modes. The ejecta can take the form of a spark shower, localized fragments, or shell ejection. The spark shower depends on particle density, while the latter two modes are based on internal cell particles released during high-speed venting. As LIB cells are closely packed, TR can easily propagate onto the neighboring cells initiating a destructive failure.

3.2. Initiation Mechanisms and Reactions

The root cause of TR is short-circuiting that results from direct contact between the battery electrodes. This contact can be internal, formed because of separator damage, or when a conductive material penetrates through the electrode layers. The resulting localized high current density causes a rapid temperature rise, initiating a series of exothermic chain reactions within the cell that further elevate the temperature to exacerbate the condition [74].

One of the first processes is the vaporization of the electrolytic solvents, elevating the internal pressure. In pouch cells, this causes visible swelling, while in cylindrical or prismatic cells, the pressure is relieved through venting. The vented gases consist of flammable organic solvent vapors, which are prone to ignition either during or after venting due to their low flash point.

Concurrently, the solid electrolyte interphase (SEI) layer decomposes, which initiates further reactions between the anode and the electrolyte. At elevated temperatures, electrolyte breakdown results in the formation of hydrocarbons and HF. Additional gases such as C_2H_4 (ethylene), C_2H_6 (ethane) and C_3H_6 (propylene) form as the solvents react with the lithium metal of the cathode [75].

Understanding the solvent decomposition mechanism is critical to understanding TR. Table 1 presents some of the dominant decomposition reactions of ethyl methyl carbonate (EMC), dimethyl carbonate (DMC), diethyl carbonate (DEC), and ethylene carbonate (EC), obtained from pyrolysis experiments.

Table 1. Decomposition reactions of different electrolytic solvents.

Solvent	Reactions #	Reaction	Type
Dimethyl Carbonate (DMC) [76]	R1	DMC $\rightarrow CH_3OCH_3 + CO_2$	Unimolecular
	R2	DMC $\rightarrow CH_3 + CH_3OC(=O)O$	Unimolecular
	R3	DMC + H $\rightarrow H_2 + CH_3OC(=O)OCH_3$	Bimolecular
	R4	DMC + $CH_3 \rightarrow CH_4 + CH_3OC(=O)OCH_2$	Bimolecular
Ethylene Carbonate (EC) [77]	R5	EC $\rightarrow CH_3CHO + CO_2$	Unimolecular
	R6	EC $\rightarrow C_2H_4O + CO_2$	Unimolecular
	R7	EC $\rightarrow C_2H_3OH + CO_2$	Unimolecular
Ethyl-methyl Carbonate (EMC) [78]	R8	EMC $\rightarrow C_2H_4$ + COC*OOH	Unimolecular
	R9	COC*OOH $\rightarrow CH_3OH + CO_2$	Unimolecular
Diethyl Carbonate (DEC) [79]	R10	DEC $\rightarrow C_2H_5OC(=O)OH + C_2H_4$	Unimolecular
	R11	$C_2H_5OC(=O)OH \rightarrow C_2H_5OH + CO_2$	Unimolecular

Sun et al. [76] reported that DMC undergoes four dominant unimolecular decomposition pathways between 500 and 2300 K, as shown in Table 1. These include the formation of dimethyl ether (CH_3OCH_3) and carbon dioxide (CO_2) formed via R1. Bimolecular pathways such as R3 and R4 become increasingly favorable at higher pressures. Similarly, DEC is transformed into diethyl ether (C_2H_5OH), ethylene (C_2H_4), and CO_2 at temperatures between 700 K and 1200 K. Other reaction pathways that are not included in Table 1 are possible at higher temperatures.

For EC, Kanayama et al. [77] identified R5 as the dominant pathway (300–3000 K), forming acetaldehyde (CH_3CHO) and CO_2, likely due to its lower activation energy. Takahashi et al. [78] studied EMC and found that it forms methoxy formic acid (MFA, COC*OOH) and C_2H_4 around 850 K, with MFA further decomposing to methanol (CH_3OH) and CO_2

at the same temperature. At 1050 K, secondary decomposition products such as carbon monoxide (CO) and CO_2 were also observed.

In addition to the electrolyte, the cathode material begin decomposing at temperatures between 200 and 600 °C [80], releasing oxygen due to its lithium oxide content. This oxygen acts as an oxidizer, sustaining combustion [75]. Each cathode chemistry influences TR differently, so individual decomposition pathways are not detailed here. For example, comparative experiments reveal that NMC-based cells emit higher volumes of hazardous gases and propagate TR more readily than LFP cells, indicating chemistry-dependent risk profiles [81].

The severity of TR depends on both the total energy stored in the battery and the magnitude of current through short circuits. Electrolyte and cathode decomposition supply the fuel and oxidizer required to sustain a fire, while the heat generated from the short circuit during TR completes the fire triangle. A self-sustaining fire alongside toxic emissions makes LIB fires incredibly difficult to extinguish [82,83].

3.3. Thermal Runaway Triggers

TR can be induced by many factors, including internal manufacturing defects as well as external triggers such as overheating, overcharging or mechanical damage [67,83,84]. Generally, overheating can cause the separator to shrink or melt, increasing the risk of internal short circuits [71,85]. Meanwhile, overcharging, which occurs when a battery is charged beyond its cutoff voltage or 100% SOC, leads to lithium plating on the anode. Over time, these lithium deposits may form dendrites that could pierce the separator and initiate internal shorts [86,87]. Overcharging can also increase the internal cell temperatures, accelerating the decomposition reactions described earlier, and heightening TR risk.

Mechanical damage can be caused by external events such as vehicle collisions or internal processes like vibration-induced micro-cracks in the separator [88]. Manufacturing impurities and lithium dendrite growth during regular operation are also known contributors to separator damage [83,89]. In EV packs, where many cells are interconnected, the failure of even a single cell can lead to TR propagation [90,91]. The intense heat during a TR, sometimes as high as 700 °C, can easily spread to neighboring cells and modules [92].

3.4. Accelerated Testing of LIBs: Nail Penetration and Thermal Abuse Tests

Due to hazards associated with TR, regulatory bodies increasingly require manufacturers to perform comprehensive safety testing of LIBs before commercialization [93,94]. However, real-world TR events are complex and challenging to replicate due to system scale and associated risks [95]. For instance, the Federal Aviation Administration (FAA) has reported an average of about 1.4 fires per week caused by the LIBs transported through aircraft cabins in the year 2025 [96]. In another instance, a damaged e-bike battery pack caught a building on fire [97]. Replicating such real-life scenarios can be challenging because failure events vary. Manufacturers, therefore, develop accelerated testing protocols by raising the stress factor levels on the LIBs to hasten degradation levels [98].

In real-world applications, LIBs may be exposed to thermal, electrical, and mechanical damage [99]. Failure testing protocols must, therefore, replicate these scenarios. On the one hand, NP tests are a standard mechanical abuse test, simulating failures like those in vehicle crashes where sharp objects may penetrate the cell [100–103]. A conductive nail in NP tests can create contact between the electrodes forming a conductive path that induces a short circuit [104,105]. On the other hand, in TA tests, cells are subjected to sustained elevated temperatures to simulate overheating conditions, or directly exposed to an external flame or fire to represent extreme thermal environments such as those encountered during vehicle or pack-level fires [106,107].

Both NP and TA tests have become two important lab tests in battery safety research, and the results are influenced by factors such as battery types and test conditions. Abaza et al. [108], for example, found that using conductive nails in NP tests causes greater temperature spikes than non-conductive ones. The emission profiles between NP and TA can also differ when compared to one another. A study comparing various TR initiation methods found different quantities and concentrations of emitted gases even for the same cell chemistry [101]. Sections 4 and 5 of this work discuss the details of NP and TA, respectively. A summary of different abuse test methods for LIBs is provided in Table 2. Each method sheds light on specific failure mechanisms, supporting a systematic exploration of real-world abuse conditions that can compromise LIB safety.

Table 2. Abuse test methods for LIBs [109–111].

Abuse test	Test Type	Description
Oven test	Thermal	The cell is exposed to prolonged, elevated temperatures, simulating thermal stress.
Fire test	Thermal	The cell is subjected to direct exposure to an external flame or fire, simulating extreme heat conditions.
External short-circuit test	Electrical	The cell's terminals are shorted with a low-resistance conductor, resulting in a rapid discharge.
Overcharge test	Electrical	The cell is charged beyond its designated cutoff voltage, reaching a predetermined state of charge (SOC) beyond safe limits.
Nail penetration test	Mechanical	An object pierces the cell, creating an internal short circuit that leads to rapid discharge and potential failure.
Crush test	Mechanical	The cell is subjected to mechanical compression, causing internal damage that leads to short-circuiting and rapid discharge.

3.5. Emissions and Safety Implications in Abuse Tests

Emissions are a major concern during battery TR tests due to the release of combustible and toxic gases. The initial venting of these gases can begin before TR initiation, and may continue after TR, posing risks to both humans and infrastructure. Accurate quantification of these emissions is therefore essential. Studies have identified various flammable organic solvents such as EMC, DEC, and EC, and hazardous gases such as benzene, toluene, CO, CO_2, and HF [104]. In a related work, Sandia National Laboratories found that ethyl-based solvents (e.g., EMC) released more flammable gases such as hydrogen (H_2) compared to methyl-based solvents, highlighting the role of solvent chemistry in TR severity [112].

Given the rapid expansion of the LIB industry and the widespread use of these batteries in high-risk applications, it is essential to perform rigorous safety assessments of the emissions from LIBs during TR events. While the emission characterization from NP and TA tests is summarized in their respective sections, Section 6 will provide a general discussion on the health and safety impact of LIB failures.

4. Nail Penetration Testing of Lithium-Ion Batteries: Mechanisms, Parameters, and Emission Profiles

4.1. Nail Penetration Test Methodologies

Nail penetration (NP) tests are usually performed in an NP test rig housed in a fire-proof and explosion-proof chamber. First, LIB cells to be tested are placed on an insulation plate in the test rig, as illustrated in Figure 3, where a cylindrical cell is used as an example. The cells need to be securely positioned between a dedicated fixture so that they don not move during NP tests. The enclosed test chamber is generally capable of withstanding LIB fires to a certain degree. A well-designed chamber can maintain a controlled atmosphere (usually inert). The emission from TR tests can be extracted using gas sampling lines in the chamber or from the exhaust. As the test parameters can significantly influence the test outcomes, well-defined methodologies are essential to ensure both reproducibility and the collection of meaningful data from NP tests. In this section, NP studies reported in the last decade are reviewed with a specific focus on the characterization of the generated emissions.

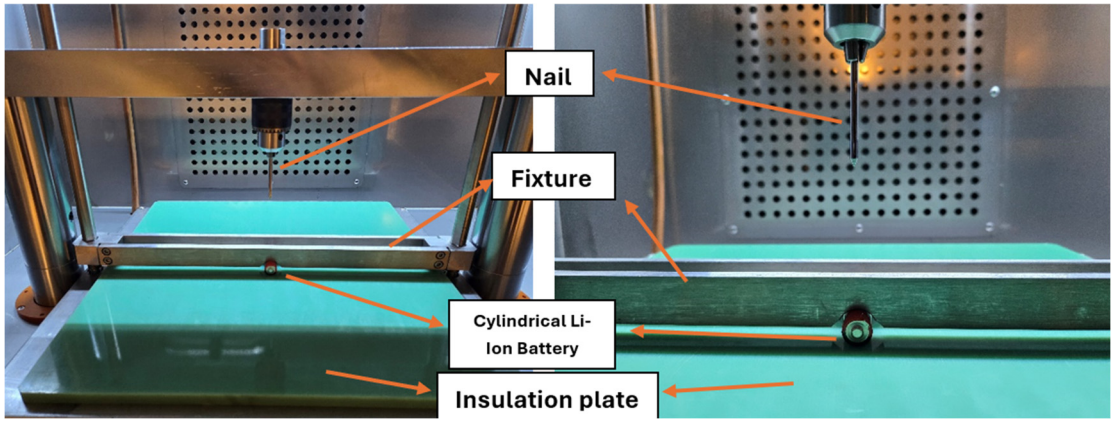

Figure 3. Photos from two angles of a nail penetration (NP) test example rig. A cylindrical Li-ion battery is used as an example.

One of the earlier studies on LIB TR emission characterization was conducted by Nedjalkov et al. [104]. They tested NMC pouch cells within a plastic barrel, and the exhaust followed a series of filters and analytical instruments installed downstream for characterization. A common configuration as such has been employed in several studies where the cells are enclosed in a chamber, and the emissions are directed into an analyzer. Koch. et al. [102], for instance, tested LIB modules in an aluminum housing. The modules have similar cathode chemistry but different capacities.

Test procedures of NP experiments are designed to obtain varying test objectives, which are seen throughout the works reviewed. For example, although both Koch et al. [102] and Nedjalkov et al. [104] examined NMC pouch cells, their objectives differed and hence, the test procedures were different. Nedjalkov et al. focused on emission characterization, and prevention methods of toxic gases using filters, whereas Koch et al. aimed to assess the effectiveness of sensors in TR detection. As a result, their procedures also varied. Nedjalkov et al. slightly overcharged (above 100% SOC) the cells to ensure TR, while Koch et al. preconditioned the cells to 60 °C and full SOC before initiating NP.

Preconditioning the cells prior to testing is an important step in NP experiments, as the cell condition could lead to different NP results. Diaz et al. [113] performed a comprehensive analysis of LIB NP by comparing emissions across multiple cell chemistries and formats, including LCO, LFP, and NMC cells in both cylindrical and pouch configurations. A nitrogen (N_2)-filled chamber was used with gas analyzers positioned downstream. Un-

like earlier studies, they did not overcharge or preheat the cells, which resulted in several 50% SOC cells failing to undergo TR.

Special cell fixture designs may be required to obtain a more precise emission characterization. For example, Essl et al. [101] adopted a more advanced chamber design to test pouch and prismatic NMC cells. The test configuration was similar to that of Diaz et al. [113] and Nedjalkov et al. [104], but great importance was placed on the design of the cell fixture. The custom-designed chamber consisted of two stainless steel holders for the cell, separated by mica sheets to prevent any thermal conduction to the test rig. It was pressure-sealed and filled with N_2. Gas sensors were placed inside the chamber in addition to other analytical instruments positioned downstream of the chamber. Compared to the plastic barrel setup used by Nedjalkov et al. [104], where no carrier gas was reportedly used, the controlled chamber environment used by Essl et al. [101] and Diaz et al. [113] allowed a more precise emission characterization.

Different experimental approaches have been developed to study emissions during NP-induced TR. Hoelle et al. [114], for instance, used an autoclave calorimeter to test NCA and NMC prismatic cells under tightly controlled conditions. The cells were wrapped on all sides using copper blocks to restrict expansion and isolate heat transfer, allowing a detailed assessment of mass loss and heat generation during TR. Although the study tested 50 cells in total, only the emissions from one out of the 50 samples were analyzed, limiting the generalizability of the observations.

Environmental and testing conditions have been shown to significantly influence both the onset and severity of TR, including the emission characteristics. Doose et al. performed NP tests in sealed chambers equipped with humidity-controlled bubblers and voltage-dependent nail control, and the nail movement was automatically halted upon voltage drop, thereby improving the reproducibility of short-circuit initiation [103]. This configuration was utilized in another study by Diekmann et al. to assess the impact of nail geometry on TR behavior, with some tests following the SAE J2464 protocols to ensure procedural consistency [115].

While most emission studies of NP have relied on closed systems to minimize ambient contamination and ensure accurate sampling, open-air configurations have also been explored in some studies. In one such study, Willstrand et al. [105] tested NMC prismatic cells in both open and closed chambers. The closed chamber was a concealed pressure vessel with inert N_2, and the emissions from TR were left to accumulate within the chamber making it possible to assess the generated gas volume. In the open configuration, the test rig was placed under a fume hood, with insulation panels directing the gaseous emissions upward for sampling. Although the design introduces a greater operational risk, it offers a realistic scenario of TR events. Similar open-air testing was conducted in another study involving modular LIBs, where the goal was the characterization of PM and emissions [81]. For this purpose, a comprehensive array of particle analyzers and emission samplers was integrated into the test rig. In both cases, however, emission sampling becomes more challenging due to diffusion and varying ignition behaviour of the cells under TR. More recent comparative studies by Howard et al. employed both open-configuration NP testing and sealed pressure vessel configurations to test NMC and LFP chemistries. In the open configuration, the test rig was exposed to the atmosphere, and the gas samples were collected through a sampling vent. In the closed configuration, a pressure vessel was purged multiple times with inert gases (argon or nitrogen) prior to NP testing. The gas sampling was conducted only after temperatures returned to ambient inside the pressure vessel. The instruments used in sampling were calibrated for a few target gases [116,117].

Reeve et al. conducted NP tests inside a reinforced pressure vessel originally developed for closed-system failure analysis [118]. Cells were first diagnosed through cathode

verification using XRF and instrumented with surface thermocouples before being mounted in a baffle-protected holder within the vessel. The internal atmosphere was repeatedly purged with inert gas to stabilize oxygen concentrations prior to testing. TR was initiated by driving a hardened stainless-steel nail of 3 mm diameter at 10 mm/s. To ensure a homogenous environment, a fan was used to continuously mix the gases before being sampled into Tedlar bags [118].

A more advanced methodology was implemented by Walker et al. in a large-format fractional thermal runaway calorimeter (L-FTRC) designed to quantify total and fractional heat output from large-format prismatic cells while maintaining flight-representative mechanical constraints as the cells tested were designed for satellite use. The cells were penetrated using a tungsten nail and the emissions were directed into an argon purged collection system [119].

In summary, methodological differences have been observed across recent NP studies. To ensure reliable and reproducible results, several factors must be carefully controlled. These include cell parameters such as capacity, SOC, and cathode chemistry, which significantly influence TR behavior, as well as test conditions and rig design, which determine the accuracy of measurements and the likelihood of ignition. Closed chambers enable precise quantification of vent-gas composition and mass loss, while open-air configurations offer clearer visualization of TR dynamics but are highly susceptible to ignition. Maintaining consistency in both the relevant cell parameters and the experimental conditions is essential for generating comparable NP data.

4.2. Observations During Nail Penetration-Triggered Thermal Runaway

The outcomes of LIB NP-experiments vary significantly as they are largely influenced by cell parameters and are highly susceptible to test conditions. Generally, a drop in cell voltage is observed immediately after NP, followed by a rise in cell temperature [103]. This is typically followed by the venting of ejecta, which results from internal gas generation and the subsequent pressure increase [114]. In some cases, venting can lead to cell rupture and fire [104]. At the cell-level, differences in NP outcomes are more apparent. For example, Reeve et al. [118] reported that cylindrical cells failed at the vent cap or positive terminal during other abuse tests, but not during NP. This is likely due to the alternative venting path created during the nail insertion.

The comparative study by Essl et al. [101] on pouch and prismatic cells found that hard-case prismatic cells could withstand a higher internal pressure (i.e., 855 kPa) before venting, compared to pouch cells (411 kPa). As the tests were conducted in an inert atmosphere, no fires were reported. In contrast, Diaz et al. [113] observed that some pouch cells underwent severe TR under inert conditions, leading to the melting of the cell casing, while others only experienced swelling. SOC played a significant role in the NP results: for cells at 50% SOC, only visible swelling was observed, while cells at higher SOCs had TR triggered by NP.

Diekmann et al. [115] reported that vent gases ignited under an oxygen-rich atmosphere, while under inert nitrogen, the ejecta glowed but did not ignite. Meanwhile, Willstrand et al. [105] found inconsistent ignition results when testing cells in open configuration, some ignited even at low SOCs (25%), while others did not. The cause of this disparity is unclear, but it had a direct effect on gas emissions, particularly CO_2 and CO concentrations. Cells that ignited released greater amounts of CO_2.

Later studies suggest that NP test outcomes are influenced by the cathode chemistry [116,117], as is evident from the NP tests performed on LFP and NMC pouch cells. The LFP cells did not show any signs of TR, and only a slight swelling was observed in the NMCs. In contrast, another recent work discovered that fully charged pouch cells behaved

differently under inert conditions despite identical cathode chemistries [120]. The cell with lower capacity and volume was found to undergo a more severe TR, marking a disparity with previous findings.

These studies collectively show that NP-induced TR outcomes are highly inconsistent across the literature due to variations in cell parameters, cathode chemistry, and the test environment. As a result, findings often appear contradictory: some studies report no ignition under inert conditions, while others observe severe TR; some cells rupture dramatically, whereas others only swell, and even cells with identical chemistries can behave differently depending on capacity and construction.

The key message of this section is that NP outcomes cannot be generalized across studies. Instead, they depend strongly on the specific interplay between the cell properties and the experimental setup used. Understanding these dependencies is essential before drawing conclusions or comparing results across NP investigations.

4.3. Influence of Cell Parameters on NP Results

4.3.1. Cell Capacity

Cell capacity is a key parameter in determining the TR hazard during NP tests, because of the total stored energy within the cell that can intensify the heat generation during an induced short-circuit.

Results from Nedjalkov et al. [104], Essl et al. [101] and Premnath et al. [81] can be compared to demonstrate the effect of capacity on NMC pouch LIB NP test results using varying methodologies. Nedjalkov et al. [104] conducted tests on 40 Ah cells in a sealed chamber with comprehensive analytical tools. Their results revealed a wide range of emission species, including multiple hydrocarbons, solvent vapors, and alcohol compounds. However, Essl et al. [101] and Premnath et al. [81] used slightly higher capacity cells (58–65 Ah/cell), and detected various other hydrocarbons in the emissions from NP tests. A detailed list of emission species can be found in Table 3. The findings from all three studies, however, do not completely overlap, which islikely because they were influenced by their test setups and environments. Premnath et al. [81] performed NP on modular LIBs in an open setup, but Essl et al. [101] and Nedjalkov et al. [104] conducted cell-level experiments in enclosed chambers. In addition, an inert atmosphere was maintained in the chamber in [101], while no such measures were taken in [104].

Table 3. Studies focused on LIB nail penetration tests and emissions analysis.

Study	Battery Type	Capacity	Test Environment	Analytical Tool	Maximum Temperature Measured	Gases Detected
2016: Nedjalkov et al. [104]	NMC Pouch Cell	40 Ah	Plastic Barrel with multiple filters downstream (non-inert)	GC-MS: Gas Chromatography Mass Spectrometry QMS: Quadrupole Mass Spectrometry QEPAS: Quartz-Enhanced Photoacoustic Spectroscopy IC: Ion Chromatography	Temperature not reported	GC-MS: Benzene, Toluene, Styrene, Biphenyl GC-MS: EC, EMC, DEC QMS: H_2, H_2O, N_2, CO, O_2, Ar, CO_2, COS, SO_2, ClO_2, Fluoroform, Benzene, Toluene, Acrolein IC: HF

Table 3. *Cont.*

Study	Battery Type	Capacity	Test Environment	Analytical Tool	Maximum Temperature Measured	Gases Detected
2018: Koch et al. [102]	NMC Pouch Modules 1: Energy density of 700 Wh/L, One module 2: Energy density of 540 Wh/L, Two modules	1: 65 Ah/cell 2: 58 Ah/cell	Aluminum housing (non-inert)	Gas Sensors	1: 200 °C 2: ~370 °C	CH_4 and/or C_3H_8 and/or CO
2018 Diaz et al. [113]	1: LCO Pouch cell 2: LFP 18650 3: LCO 18650 4: NMC 18650	1: 2.5 Ah 2: 1.1 Ah 3: 3.0 Ah 4: 2.6 Ah	Test chamber with air (non-inert) and nitrogen atmosphere (inert)	FTIR O_2 Analyzer H_2 Analyzer Ion Chromatography coupled with plasma optical emission spectrometry	For LCO pouch cell, temperature > 700 °C at 100% SOC	Only emissions from pyrolysis were reported. These included EC, DMC, PC, DEC, HCl, CO, Acrolein, COF_2, HF, Formaldehyde (CH_2O)
2020: Essl et al. [101]	1: NMC Pouch 2: NMC Prismatic	1: 60 Ah 2: 60 Ah	Stainless steel reactor with nitrogen atmosphere (inert)	FTIR coupled with GC	1: Pouch: Max surface temperature: 783 °C 2: Prismatic: Max surface temperature:743 °C	1: Pouch: H_2, C_2H_4, CH_4, CO, CO_2, H_2O, C_4H_{10} 2: Prismatic: H_2, C_2H_4, CH_4, CO, CO_2, DMC, H_2O, C_4H_{10}
2020: Diekmann et al. [115]	LNCO/LCO Pouch cell	5.5 Ah	Test chamber with air (non-inert) and nitrogen atmosphere (inert)	FTIR	Max surface temperature: ~500 °C	H_2O, CO_2, CO, CH_4, C_2H_6, C_2H_4, HF, EMC, EC
2021: Hoelle et al. [114]	1: NCA Prismatic 2: NMC Prismatic	8 Ah to 145 Ah	Autoclave calorimeter with argon atmosphere (inert)	GC	-	H_2, CO, CO_2, CH_4, C_2H_4
2021: Doose et al. [103]	LNCO/LCO Pouch cell,	3.3 Ah and 5.3 Ah	Steel chamber with nitrogen atmosphere (inert)	FTIR	1:Max. Cell surface temperature 521 °C 2: Max. Cell surface temperature 533 °C	From both the cells: C_2H_4, C_2H_6, CO, CO_2, EC, EMC, HF
2022: Walker et al. [119]	LSE134-LCO cathode	>100 Ah	Large format—Fractional Thermal Runaway Calorimeter with argon atmosphere (inert)	GC-FID	Vent gas temperature ~65 °C	CO_2, H_2, C_2H_6, O_2, CH_4

Table 3. *Cont.*

Study	Battery Type	Capacity	Test Environment	Analytical Tool	Maximum Temperature Measured	Gases Detected
2022: Premnath et al. [81]	MODULES 1: LFP cylindrical 2: NMC pouch	1: 2.3 Ah 2: 60 Ah	Open-air setup (Non-inert)	FTIR	1: LFP: Max. cell surface temperature of 85.5 °C 2: NMC: Max. cell surface temperature of 900 °C	1: LFP: CO_2, CO_L, CH_2O, NO, NO_2, HCl, HF, HCN, CH_4, C_3H_8 2: NMC-higher concentrations of: CO_2, CO_L, CH_2O, NO, NO_2, HCl, HF, HCN, CH_4, C_3H_8,
2023: Willstrand et al. [105]	NMC Prismatic cell	157 Ah	1: Closed pressure vessel with nitrogen atmosphere (inert) 2: Open-air setup (non-inert)	FTIR, FID, Micro-GC	Max cell temperature 665–857 °C	CO, CO_2, H_2 (average from all the tests)
2025: Reeve et al. [118]	NCA cylindrical 21,700 cell	4 Ah	Sealed vessel with argon atmosphere (inert)	Mass Spectrometry (MS)	465–665 °C	H_2, CO_2, CO, C_2H_6, C_2H_4, C_3H_8, C_3H_6, CH_4
2025: Howard et al. [116,117,120]	1: LFP Cylindrical cells 2: LFP pouch and prismatic cells 3: NMC pouch cells 4: NMC pouch cells	1: 3 Ah 2: 50 Ah and 105 Ah (Prismatic); 25 Ah (Pouch) 3: 5 Ah 4: 10 Ah, 15 Ah, and 30 Ah	1: Pressure vessel with nitrogen or argon atmosphere (inert) 2: Open-air setup (non-inert) 3: Pressure vessel with nitrogen and air atmosphere (inert and non-inert) 4: Pressure vessel with nitrogen or argon atmosphere (inert)	QMS and FTIR	1: 98–260 °C 2: 21 °C and 46 °C (Prismatic); 19 °C (Pouch) 3: 1010–1038 °C 4: Maximum cell surface temperature 10 Ah: 584–736 °C 15 Ah: 14–36 °C 30 Ah: 142–261 °C	1: H_2, CO_2, CO, C_2H_6, C_2H_4, C_3H_8, C_3H_6, CH_4 2: N/A 3: H_2, CO_2, CO, C_2H_6, C_2H_4, C_3H_8, C_3H_6, CH_4 4: H_2, CO_2, CO, C_2H_6, C_2H_4, C_3H_8, C_3H_6, CH_4

The results for NMC prismatic cells can be compared in Essl et al. [101], Hoelle et al. [114], and Willstrand et al. [105]. Hoelle et al. explored a broad range of cell capacities (i.e., 8–145 Ah), while Essl et al. and Willstrand et al. tested cells at 60 Ah and 157 Ah, respectively. According to these studies, the total gas generation per unit capacity ranged from 1.77 to 2.06 L/Ah, suggesting a correlation between cell capacity and gas evolution. The observed variation in gas volume appears to correlate with differences in stored energy, indicating the influence of capacity on TR outcomes.

4.3.2. Test Environment

The test environment plays a crucial role in shaping TR behavior during NP experiments. Open test rigs could not control the test environment, and only a few papers reported their studies conducted in open test rigs in room air. Willstrand et al. [105] observed that cells tested in open configurations had slightly lower TR onset temperatures compared to those in closed and inert chambers. The temperatures ranged between 130 °C and 210 °C depending on the SOC. Notably, fires were initiated at SOCs as low as 25% in the open tests, suggesting increased flammability under these conditions. Similarly, Premnath et al. [81] reported fires in most of their NP test cases of battery modules in an open rig. The fires occurred due to the readily access of air in the open rig setup, and the high energy content in the battery modules also contributed significantly to the larger fires and greater quantities of combustible gases emitted. However, an LFP module that underwent NP tests was reported not catch fire [81]. The fact that LFP cells are difficult to ignite was also confirmed in Howard et al. [116], where LFP cells of different capacities were found not to undergo failure during NP tests, let alone a TR.

Most closed-chamber experiments were conducted in inert atmospheres such as nitrogen or argon, which may suppress ignition during NP tests. However, Diekmann et al. [115] noted that the use of oxygen-filled atmosphere can create overpressure conditions within the chamber, which may influence the TR onset. In their comparative study on LCO pouch cells using compressed air and N_2 in a closed chamber, they observed ignition events only in NP tests in air-filled chambers, along with a notable spike in short-term pressure. The pressure was approximately 1.48 bar during the deflagration in air, while it was only half as much ina N_2-filled chamber. Interestingly, the maximum TR temperatures remained similar across tests conducted in both atmospheres. This may suggest that the observed differences in TR temperatures for tests conducted in open and closed chambers in [105] may be due to the confinement conditions rather than to the gas composition alone.

Gas production rates differ in tests conducted in different environments, e.g., air, inert, or humid N_2, but different trends are reported in the literature. For example, Diaz et al. [113] found that inside the enclosed test chamber, using air as a carrier gas for the TR emissions resulted in measuring greater emission volumes than when N_2 was used as the carrier, indicating that the oxidative environment may enhance gas generation. In contrast, a different trend was reported in [117] where an average net gas volume of 10.7 L was emitted in a N_2 atmosphere, and only 8.9 L was emitted in the presence of air. In this study, they used a pressure vessel for NP. Another study uniquely incorporated humidity control into its chamber design using a bubbler system. Their results showed that increased humidity within a N_2 environment promoted condensation of vapour-phase products on chamber surfaces, reducing the concentration of measurable gaseous species [103].

In summary, these studies demonstrate that while inert environments may not significantly alter TR temperature thresholds unless coupled with pressure effects, they do influence the total gas generation and combustion behavior. Therefore, variables such as confinement, oxidizing atmosphere, and humidity should be carefully considered when designing NP test environments. Results obtained in different gas environments should also be compared with special care.

4.3.3. Nail Characteristics

The influence of nail characteristics in NP tests can be analyzed from two perspectives. The first are the operational parameters, including the penetration speed and depth of insertion, while the second involves the geometry and material of the nail, such as diameter, tip angle, and conductivity.

Nail penetration speed can impact the reproducibility of NP results. Diekmann et al. [115] examined the influence of penetration speed (e.g., 1 mm/s, 5 mm/s, 10 mm/s, 40 mm/s, and 80 mm/s) and found that using a penetration speed of 1 mm/s, much lower than the 80 mm/s suggested in SAE standards, could significantly lower standard deviations in temperature and voltage profiles. This slow penetration rate was found to be able to allow for more stable and consistent triggering of TR [115]. This low penetration speed (i.e., 1 mm/s), was later adopted by other researchers, such as Doose et al. [103].

The penetration speed also appeared to play a role in the composition of solvent vapor in the emissions from NP tests, which was found to be impacted by the residence time. Faster penetration rates (e.g., 80 mm/s) may limit the residence time required for intermediate reactions, leading to a higher fraction of unreacted solvent vapors in the final emission mixture. This may also explain the reason why low penetration speeds produce more reproducible results, as the generated gases get almost equal residence time before venting [115].

In addition, one might expect that increasing the diameter of a conductive nail would allow higher short-circuit currents, potentially intensifying the TR event. However, based on a NP study on LCO cells using various nail diameters (i.e., 2–5 mm) and tip angles (i.e., 20–40°) [103], it was found that nail geometry did not significantly affect whether TR occurred or how severe it was. The authors attributed the outcomes to the dominant influence of the low penetration speed (i.e., 1 mm/s), which may limit short-circuit current regardless of nail size. More studies are needed to confirm this.

In terms of nail material, Diekmann et al. [115] noted that using conductive nails as opposed to non-conductive ones enhanced reproducibility. Conductive nails directly contact the electrodes during penetration, ensuring a short-circuit event, whereas non-conductive nails may not directly connect the internal layers, delaying or weakening the trigger.

Based on these findings, recent studies focusing on characterizing the emissions from NP tests tend to fix nail characteristics (especially penetration speed) to ensure consistent TR triggering in the tests [116,117]. However, the influence of nail material and shape under different conditions, such as faster penetration speeds or varying cell chemistries remains underexplored.

Overall, these findings suggest that while slow penetration speed and conductive nails are preferred in NP tests to enhance the reproducibility, the role of geometry in influencing TR is not yet conclusive. Further studies are needed to determine whether these observations hold true across cell formats, SOC levels, and more sophisticated test setups.

4.3.4. State-of-Charge (SOC)

The state-of-charge (SOC) plays a critical role in determining the likelihood and TR severity during NP. Most experimental studies were conducted at 100% SOC, as this condition is more likely to trigger TR and allow researchers to assess the worst-case scenarios [102,104,116]. Conducting NP tests on fully charged batteries seems to become a standard practice in the literature.

However, there are a few studies that explored the SOC effects on NP results, such as [113] and [105]. Diaz et al. [113] performed NP on LCO pouch cells in an open environment, and they found that only cells with 100% SOC experienced TR during NP tests, while the cells at 50% SOC exhibited only swelling and gas release but did not enter runaway. A more recent study also observed that only NMC pouch cells at full charge experienced TR conditions during NP tests regardless of the test environments [117]. On the other hand, Willstrand et al. [105] used a closed chamber setup and tested high-capacity NMC prismatic cells. They observed TR for cells at both 25% and 100% SOCs, while the peak temperature

during TR was significantly higher for cells at 100% SOC. This suggests that while TR can still occur at lower charge levels in large-format cells (e.g., prismatic), the severity of the event increases with SOC.

Overall, these findings highlight that batteries with different SOCs can demonstrate different TR behaviors, but the impact of SOCs is also intertwined with cell format, capacity, and the test environment. Future studies that decouple these variables could provide more generalized insights into the SOC-TR relationship.

4.4. Temperature Measurement in Nail Penetration Tests

Temperature is a key indicator in TR studies, as it informs the design requirements for the thermal protection systems capable of withstanding high heat fluxes from cell surfaces and vent emissions. Temperature profiles during NP tests are usually measured using thermocouples, but different placement strategies exist based on the test setup and objectives of the study. For example, Koch et al. [102] positioned a K-type thermocouple on the module surface near the NP site, likely aiming to capture an average surface temperature, while Essl et al. [101] placed thermocouples at multiple points, including the cell surface and tabs, sandwiched between insulation sheets. This multi-thermocouple setup enabled them to isolate the peak cell temperature from the vent gas temperature, an advantage in detailed thermal characterization.

Closed-chamber setups impose constraints on thermocouple placement due to space limitations, whereas open setups provide greater flexibility for thermocouple placement. For example, Premnath et al. [81] installed 15 thermocouples around the module and an additional six inside the exhaust duct, including one for measuring ambient temperature. Willstrand et al. [105] opted for a minimal configuration with four thermocouples: three on the cell surfaces and one on the safety vent. Others integrate thermocouples into the nail itself to monitor internal cell temperature during penetration, helping them highlight a correlation between nail depth and TR severity [115].

While most studies rely on type K thermocouples for their affordability and wide temperature range, type N thermocouples were also used as in [116,118,120] with an improved performance at high temperatures. However, type N thermocouples are usually at a higher price [121].

In summary, thermocouple quantity and placement are both critical. While embedding sensors inside the nail offers insight into pre-TR temperature rise, external placement near vents enables accurate tracking of emission heat profiles. Proper insulation and strategic positioning help minimize heat losses and avoid interference with the cell's failure behavior.

4.4.1. Temperature Profiles of Different Battery Types and Configurations

Temperature peaks during NP tests vary significantly based on cell chemistry, form factor, SOC, and measurement strategy depending on whether TR occurs or not. Premnath et al. [81] reported that the thermocouple located beneath the NP site consistently recorded the highest temperatures during TR. This was confirmed across multiple tests, particularly for LFP modules. Their study also highlighted the stark contrast in peak temperatures between batteries of different chemistries: NMC modules were found to reach up to 900 °C, while LFP modules peaked at only 175 °C.

The trend that LFP batteries exhibit less severe results than NMC ones during NP tests was confirmed by multiple independent studies. Howard et al. [116] reported that during NP of LFP prismatic and pouch cells, no TR, fire, or visible failure indicators such as smoke were observed. Surface temperatures for these LFP cells remained low, ranging from 19 °C to 46 °C. On the other hand, they found that the NMC cells reached a maximum temperature ranging from 1010 °C to 1038 °C under NP-induced TR [117]. This suggests

a strong thermal stability for LFP cells under NP conditions, especially when compared against chemistries such as NMC and LCO. Similarly, Essl et al. [101] reported a large temperature rise in NMC cells, with the surface temperatures reaching 782 °C for NMC pouch cells, and 777 °C for prismatic cells. However, Koch et al. [102] observed significantly lower temperatures (200–350 °C). This was because, the thermocouples in [102] were placed inside the aluminum housing without making contact with the cell surface while in [101], they were in contact with the cell surface inside the confined-inert reactor.

Vent gas temperatures can be significantly different from the surface temperature of the battery cells. For example, the pouch NMC cell emitted gases at around 356 °C during NP tests, while the vent gas from a prismatic NMC cell could reach 1035 °C, although similar surface temperatures for both pouch and prismatic NMC cells were found [101]. This disparity is likely due to structural differences: pouch cells tend to rupture and release gases more diffusely due to swelling, whereas prismatic and cylindrical cells vent through a defined burst plate, enabling more focused and measurable gas streams.

For LCO pouch cells, different temperature profiles were reported. For example, Diaz et al. [113] estimated a maximum temperature exceeding 700 °C during TR based on visual evidence of a melted aluminum casing, while Diekmann et al. [115] recorded only about 500 °C based on the measurement using a high-accuracy, glass fiber tape-insulated thermocouple. This discrepancy reflects uneven temperature distributions during NP tests and emphasizes the need for standardized, robust temperature measurement protocols in NP studies. For example, cell surface temperatures and vent gas temperatures may vary depending on the cell form factor and therefore, must be accounted for when positioning temperature sensors.

4.4.2. Influence of Test Environment on Thermal Runaway Temperatures

The surrounding environment plays a critical role in determining the temperature profile of LIBs during NP tests, but this factor remains underexplored in many studies. Willstrand et al. [105] observed that ambient conditions significantly altered the maximum recorded temperatures. For NMC prismatic cells at 100% SOC, the ones tested in an open setup reached peak temperatures between 665 °C and 725 °C, while those tested inside a closed N_2-chamber exhibited much higher values, ranging from 838 °C to 857 °C. This suggests that heat dissipation is more constrained in a closed chamber, leading to higher localized temperatures. Although the cell chemistries differ, a comparable trend was observed in the study by Howard et al. [116], who used LFP cylindrical cells. In the inert gas environment (e.g., argon or nitrogen), cell temperatures ranged between 98 °C and 260 °C, while in air, the maximum surface temperature reached only 46 °C.

The composition of the test atmosphere has a pronounced effect. Diekmann et al. [115] reported that in a nitrogen-filled chamber, the battery only reached a maximum temperature of 47 °C, compared to 122 °C in an air-filled chamber, an 88.7% increase. This finding underscores the suppressive influence of inert gases on combustion-driven temperature rise. Despite these insights, there remains a lack of systematic data on how environmental factors like ambient temperature or humidity influence the overall temperature profile during thermal runaway. It is plausible that increased humidity in the surroundings may reduce both surface and vent gas temperatures due to enhanced evaporative and convective cooling. But more studies are needed to confirm this.

4.5. Emissions Generated from Nail Penetration Tests

Studying the emissions from NP tests can enhance our understanding of the hazardous components released in battery incidents, as NP can trigger TR or venting that generates numerous hazardous emissions from the batteries. However, it is important to note that

not all NP tests result in a TR, and this greatly influences the composition of the emitted species, even under identical test conditions [116]. When TR does occur, it results in the formation of flammable gases as discussed in Section 3.

In addition to these decomposition products, unburnt electrolyte solvents may also be released. The nature and proportion of these solvents are dependent on the specific electrolyte formulation but often consist of compounds like DMC, EC, DEC, and EMC [122]. The presence of such solvents and gases poses substantial risks not only to human health but also to the environment, due to their toxicity and flammability.

Understanding the relationship between the emitted species and factors such as battery chemistry, SOC, and test configuration is essential for risk assessment and mitigation. The section explores this connection, drawing on recent experimental studies that have characterized the emissions under varying conditions of battery design and test environments.

4.5.1. NMC Pouch LIBs

NMC pouch cells are among the most studied LIB formats and emissions from their TR events are well documented. Comparing the results from four different studies in [81,101,104,117], we found that they all reported the presence of major gaseous byproducts, including CO_2, CO, and CH_4. However, their concentrations were reported at different values. For example, Nedjalkov et al. [104] quantified CO_2 and CO concentrations at approximately 55,000 ppm each, while Essl et al. [101] reported that CO_2 was up to 30% and CO was at 22%. Another study by Howard et al. [117] found the average CO_2 concentration at 48.2% and CO at 6.6% regardless of the test environment (either air or N_2). In addition, Premnath et al. [81] reported significantly higher concentrations of CO_2 compared to CO, likely due to the more intense combustion associated with modular-level fires. In addition to CO and CO_2, CH_4 was also consistently detected but in lower concentrations compared to the other two gases. For example, both [101] and [117] quantified the CH_4 concentration in the emissions to be approximately 3 vol%.

Other gases, such as hydrogen (H_2), water vapor (H_2O), and hydrogen fluoride (HF) were also reported. For example, H_2 and H_2O were detected in [104], and quantified (23 vol% H_2 and 3 vol% H_2O) in [101]. HF was identified in both [81] and [104], but its concentrations were significantly different in the two studies: the value reported in [104] is an order of magnitude higher than that in [81]. This discrepancy may stem from several factors related to experimental conditions in the two studies: the use of different analytical techniques (Fourier Transform Infrared Spectroscopy [FTIR] vs. Ion Chromatography [IC]), variations in the test setup (open vs. closed system), and potential differences in cell design or electrolyte formulation over time. It is also possible that IC, known for its sensitivity to ionic species, is more effective for quantifying HF, as seen in [104].

In addition, there are other species, such as benzene, toluene, styrene, and biphenyl, and volatile solvent vapors such as EC, DEC, and EMC that were observed using gas chromatography–mass spectrometry (GC-MS) and quadrupole mass spectrometry (QMS) [104]. The solvents are commonly found in LIB electrolytes and reported in other studies as well [101]. Notably, alkene concentrations (e.g., styrene) were found to be of similar magnitude (slightly lower) compared to solvent vapors [104]. This was, however, not observed in the work of Essl et al. [101], where FTIR and GC were used.

Overall, while there is a broad agreement on key emission species across studies on NMC pouch LIBs, notable differences in concentration and compound diversity highlight the importance of test configuration, measurement methodology, and cell design in emission characterization.

4.5.2. NMC Prismatic LIBs

NMC prismatic batteries represent the second most frequently studied LIB format. CO_2, CO, and H_2 are identified as the primary gas-phase constituents during NP–induced TR in multiple studies [101,105,114]. Higher average volumetric concentrations of these gases were reported in [114], compared to those in [101], which is likely due to the larger capacity cells used in the former study. When NMC prismatic cells were compared with pouch cells under similar SOC and test conditions, Essl et al. [101] found no major variation in the overall gas composition. This can be seen in Figure 4.

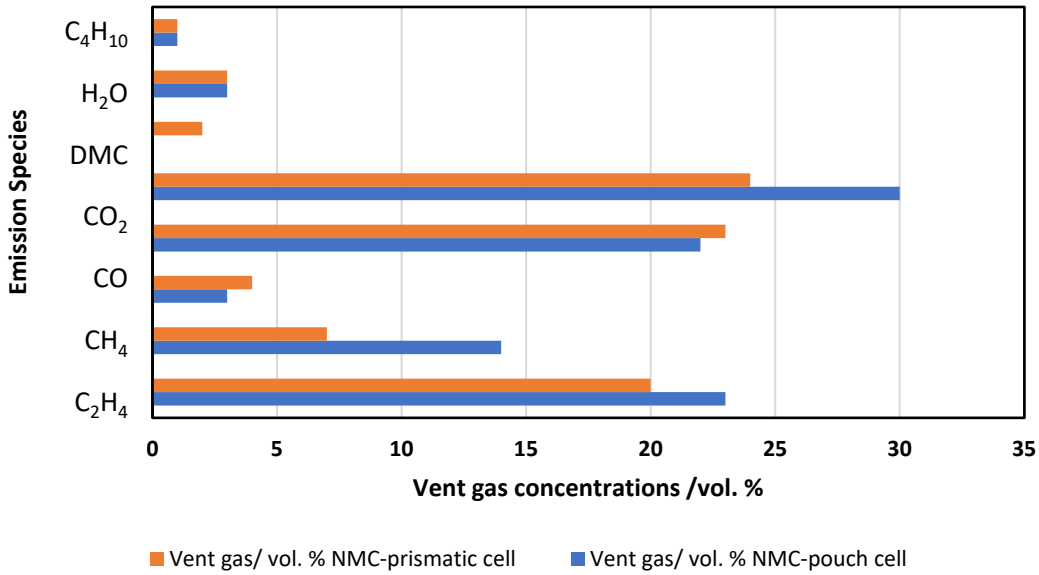

Figure 4. Vent gas composition of NMC pouch and prismatic cells. Data adapted from ref. [101].

SOC was observed to influence the relative concentrations of CO and CO_2 in prismatic cell configurations. With increasing SOC, CO concentrations became dominant over CO_2, whereas H_2 concentrations showed a more gradual increase with SOC, almost evening out with the CO_2 concentration at 100% SOC [105]. Minor hydrocarbons such as C_2H_4 and CH_4 were also detected in low concentrations in both [101] and [114]. Additionally, H_2O, butane (C_4H_{10}), and DMC were identified in the gas mixtures, typically within the 1–3 vol% range [101].

4.5.3. LCO LIB Cells

The emissions from NP-induced TR in LCO batteries were investigated in [103,113,115,119]. Emissions from both NP and pyrolysis tests were reported in [113], but the NP tests generated comparatively lower emission yields, as presented in Table 3.

Cells with different capacities were tested, ranging from pouch cells with 3.3–5.5 Ah [103,115] to prismatic cells with much larger capacities (>100 Ah) [119]. Consistent chemical species such as CO_2, CO, C_2H_6, C_2H_4, HF, EC, and EMC were detected in both [103] and [115]. Doose et al. [103] reported nearly equivalent levels of CO and EMC concentrations in the emission mixture, a result validated across four independent test runs. Diekmann et al. [115] reported the presence of EMC in the gas mixture, but did not report its concentration. In both studies, the CO concentrations, c_{CO}, ranged between 30,000 and 40,000 mg m^{-3}. Similarly, Walker et al. [119] identified an average of 3.1 L. Ah^{-1} of expelled gases containing CH_4, CO_2, C_2H_6, H_2, O_2 and N_2 within the gas mixture from their NP tests, and CO_2 and H_2 were found to dominate the emission composition.

4.5.4. Influence of Test Environment on Emissions

The test environment plays a critical role in determining the composition and quantity of emissions during TR events in NP tests. Closed-chamber experiments often incorporate an inert atmosphere to contain the emissions for accurate post-event sampling. Either argon [114,119] or N_2 [101,103,113] was used in previous studies.

The influence of environmental conditions on the emissions was explored in [115] and [117]. Diekmann et al. [115] performed testing in both N_2 and air and recommended a N_2 atmosphere for obtaining reproducible emission profiles. Howard et al. [117] conducted NP in both open (air) and closed (inert) chamber conditions to find that the total gas volume formed in air was approximately 1.3 L lower than that measured in N_2. In addition, the concentrations of H_2 and CO_2 can differ in tests conducted in air or inert environments: air environments resulted in higher CO_2 and lower H_2 concentrations, while N_2 environments produced the opposite trend as seen in Figure 5 [117].

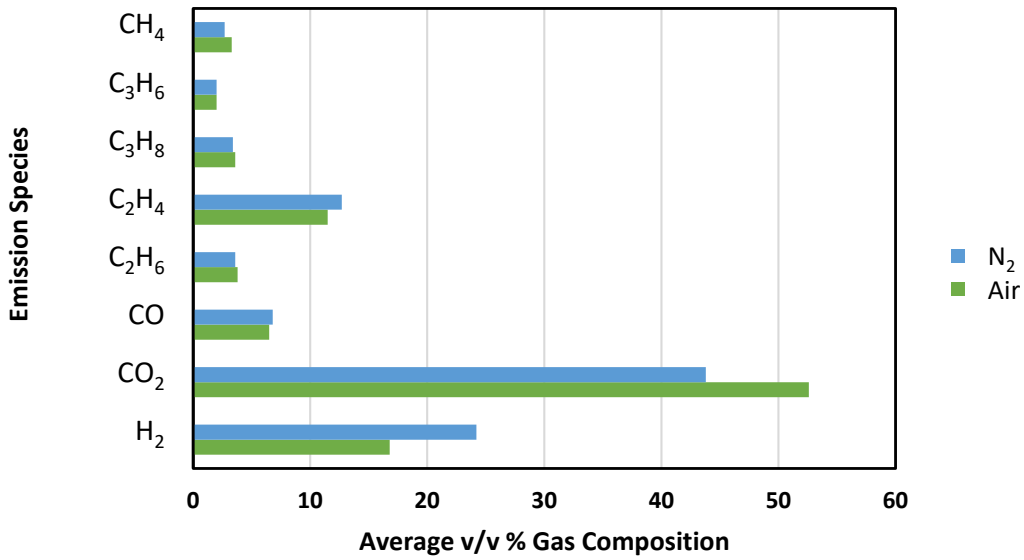

Figure 5. Influence of test atmospheres (i.e., N_2 or air) on thermal runaway emissions of 5 Ah nickel manganese cobalt oxide (NMC) pouch cells undergoing nail penetration tests at a 100% SOC. Data adapted from ref. [117].

Hoelle et al. [114] and Walker et al. [119] studied prismatic cells. Although the cathode chemistries differed, both experiments were conducted in an argon atmosphere. Walker et al. reported a high concentration of N_2 in the emissions mixture, making it the most dominant species detected. In contrast, Hoelle et al. did not observe N_2 in significant amounts. Walker et al. attributed the presence of N_2 to residual air in the chamber due to incomplete purging, despite using argon as the inert gas. In the work of Nedjalkov et al. [104], N_2 was found among the emission components, but the sampling was conducted in ambient air. Nevertheless, Walker et al. [119] suggest that even a trace of air in a closed chamber could significantly influence the resulting emission profile and complicate comparison across studies, particularly for interpreting nitrogen-bearing compounds such as NO_x.

Moreover, water vapor from the surrounding test environment may also contribute to the overall gas composition, as reported in [103]. Humidity was found to influence gas compound concentrations: tests conducted under humid conditions affected the measured concentrations, possibly due to condensation of the emission components onto the chamber surfaces. This underscores another aspect of TR emissions analysis. The influence of external test conditions, such as humidity, oxygen availability, and system openness, on emission kinetics and product distribution.

Taken together, results from [103,114,117,119] show that humidity, oxygen availability, and system openness each alter emission kinetics and product ratios in distinct ways. Humidity can influence the apparent concentrations of condensable species and contribute additional water vapor to the gas mixture, as indicated in [103]. Oxygen availability and system configuration (open vs. closed) were shown to shift the balance between CO_2, CO, and H_2, with air tests producing higher CO_2 and lower H_2 relative to inert environments, as demonstrated in [117]. Chamber integrity also plays a role, as trace air ingress during argon testing led to detectable N_2 and altered emission profiles in [119], whereas such effects were not observed under more effectively purged conditions as in [114]. Collectively, the results across these studies demonstrate that the test environment conditions are not peripheral, but critical determinants of emission profiles, highlighting the need to report them clearly when comparing NP-induced TR emissions.

4.6. Influence of Gas Collection, Analytical Techniques, and Normalization on Emission Profiles

The emission profiles reported in NP and TA studies (TA studies to be discussed in Section 5) exhibit substantial variation, which can be partly attributed to differences in gas collection methodologies, analytical techniques, and data normalization approaches. Gas collection during TR experiments is commonly performed using three main strategies: closed or sealed chambers, inert-gas-purged systems, and open or semi-open configurations. Closed and inert environments enable accumulation and post-event sampling of vent gases, facilitating quantification of total gas volumes and reducing gas species such as H_2 and CO. In contrast, open or semi-open configurations allow gas dilution and combustion in ambient air, often biasing reported emissions toward higher CO_2 fractions but lower concentrations of light hydrocarbons.

The analytical techniques employed across studies further contribute to discrepancies in reported emission compositions. FTIR is widely used for multi-gas, time-resolved measurements but has limited sensitivity for certain species such asHF. Gas chromatography-based techniques (GC, GC-MS, GC-FID) provide detailed speciation of hydrocarbons and solvent vapors but are typically applied to discrete, post-event samples rather than real-time measurements. QMS is effective for detecting light gases such as H_2 and CO but may have limitations in absolute quantification, while IC is particularly suited for capturing acidic species such as HF. Consequently, the range and relative abundance of detected species depend strongly on the chosen analytical approach.

In addition, reported emission magnitudes are influenced by differences in normalization methods. Emissions have been variously expressed as volume fractions, concentrations (ppm or mg m^{-3}), total released gas volumes, or capacity-normalized values (e.g., L Ah^{-1}). Lack of consistent normalization complicates direct comparison across studies, particularly between open- and closed-system experiments. Capacity-normalized metrics offer improved comparability by accounting for differences in cell size and stored energy, but they are not uniformly reported in the literature. These methodological and reporting variations should therefore be considered when interpreting differences in emission profiles across NP and TA studies.

5. Thermal Abuse Testing of Lithium-Ion Batteries: Mechanisms, Parameters, and Emission Profiles

5.1. Thermal Abuse Test Methodologies

Thermal abuse (TA) testing constitutes a critical methodology for assessing the safety and reliability of LIBs, particularly under extreme conditions that can precipitate TR or catastrophic failure [99,123–128]. A range of experimental approaches has been developed to replicate distinct abuse scenarios. These procedures are used to identify poten-

tial weak points and vulnerabilities in batteries, as well as to characterize safety-critical phenomena such as temperature rise, mechanical damage (e.g., swelling, venting, or rupture), and the development of hazardous byproducts such as flames, smoke, and toxic gases [99,123,126–130]. External heating is a direct TA method, which can be further divided into thermal heating and local heating [125,127].

In thermal heating, the cell or pack is exposed to controlled thermal loads in an oven or thermal chamber. The temperature inside the chamber is typically set above 100 °C, or it is gradually increased at a predefined rate (usually in increments of 4 to 5 °C) until TR occurs. On the other hand, in local heating, a specific element (such as a thermal pad or PTC heater) within the battery system is deliberately overheated. This can involve heating either one side of an LIB or an individual cell within a battery module or pack. The primary goal of this testing approach is to investigate the fire-triggered TR propagation behavior of a LIB system. In these experiments, conduction is often the dominant heat transfer mode driving the TR propagation between two cells within an enclosed battery configuration. To ensure consistency and comparability of results, TA testing protocols are frequently guided by international safety standards, including UL 1642, IEC 62133-2, and UN 38.3 [58,64,66,131].

5.2. Events During Thermal Abuse-Triggered Thermal Runaway

TR in LIBs is a complex and dynamic process involving a cascade of thermal, chemical, and mechanical events that ultimately lead to cell failure [131]. As discussed in Section 3, it can be triggered by multiple factors. This section describes the sequence of events specific to thermally induced thermal runaway (TR), where failure is initiated by external heating or fire exposure. Electrical abuse mechanisms such as overcharge and short-circuiting, which involve distinct electrochemical degradation pathways (e.g., high-voltage electrolyte oxidation, lithium plating, and cathode destabilization), are outside the scope of this section and are not discussed here.

In cases of TA, the process begins with a series of self-sustaining exothermic reactions. Initially, the SEI and separator degrade, followed by the decomposition of the electrolyte, gas generation, and a rapid, uncontrollable rise in temperature. These events lead to a violent cell failure, accompanied by the release of toxic gases, flames, and high-temperature debris [123,128,129]. The sequence of events is largely driven by temperature thresholds that trigger the exothermic breakdown of battery components. The key stages of TA-triggered TR are outlined below.

5.2.1. Initial Stages

During the initial heating phase (below 90 °C), internal components of the battery expand due to thermal effects, causing measurable strain or deformation. This physical change serves as an early warning sign of potential failure, as depicted in Figure 6. As the external temperature increases (typically between 90 and 120 °C), the SEI begins to break down [128,129]. Once TR is initiated, the flammable gases are typically expelled through the safety valve or cracks in the battery casing [111]. This increase in internal pressure leads to battery bulging and further exacerbates the progression of TR.

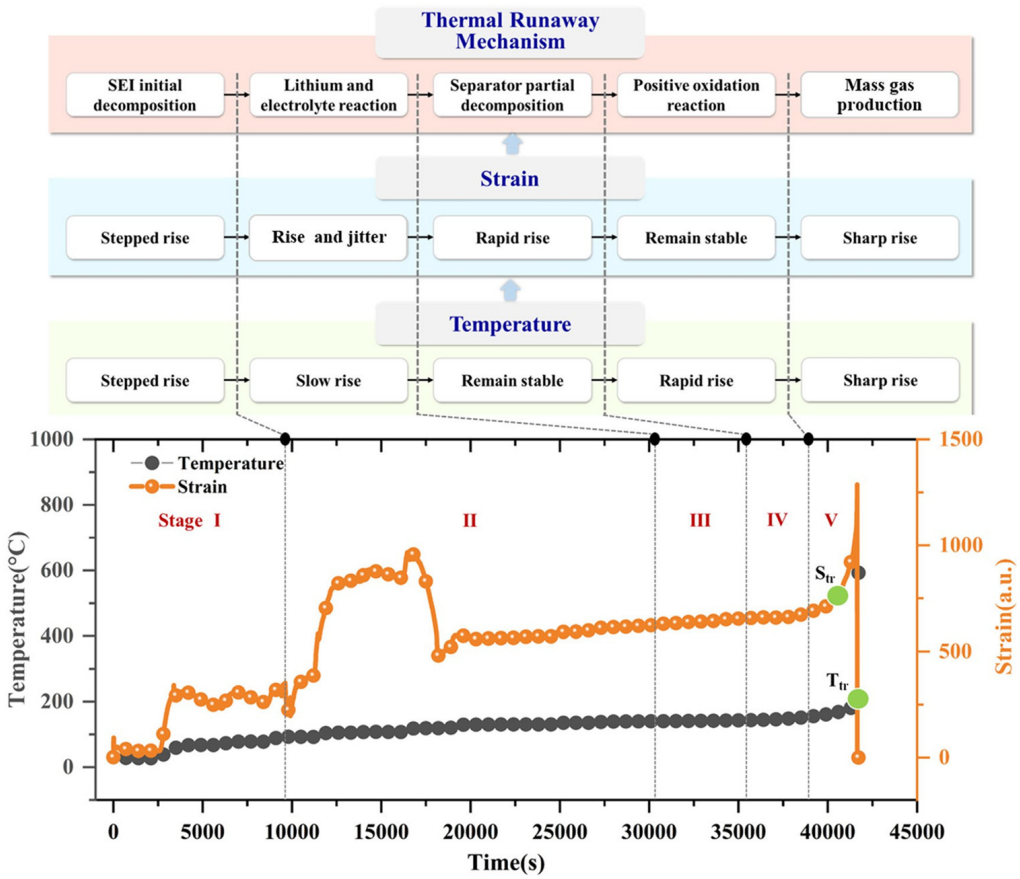

Figure 6. Strain and temperature curve during thermal abuse-triggered thermal runaway. The five stages of the process are illustrated in the upper portion of the figure. Reprinted from [123].

5.2.2. Thermal Runaway Propagation

Once the temperature reaches a critical threshold (typically around 130–150 °C), the battery enters the propagation phase [111,126,128]. Here, electrolyte decomposition, separator melting, and further exothermic reactions occur. As the temperature continues to rise, the damaged SEI layer exposes the anode to the electrolyte, triggering a chain reaction that generates more gas and heat from continued electrolyte breakdown. The electrolyte decomposes into volatile, toxic gases, including CO_2, CO, and HF [132]. These gases are both flammable and toxic, and their rapid release can cause the cell to swell or rupture. The rising temperature leads to the melting of the separator (135–165 °C), allowing the electrodes to make contact, resulting in an internal short circuit. The polyolefin-based separator melts, compromising the cell's structural integrity, which accelerates the exothermic reactions.

5.2.3. Progression to Full Thermal Runaway

As the temperature exceeds critical thresholds, exothermic chemical reactions between the cathode, anode, and electrolyte become increasingly violent. In cells with higher energy densities (such as lithium cobalt oxide (LCO) and nickel manganese cobalt (NMC) cells), these reactions release large amounts of heat, further raising the temperature and accelerating the process. As the heat generated outpaces the cell's ability to dissipate it, the temperature rises dramatically. This creates an environment where internal pressure builds, eventually causing the cell casing to rupture [126]. The release of hot, flammable gases and particles ensues. The cathode material begins to decompose, releasing oxygen, which acts as an oxidizer to fuel the fire even in the absence of external air. This newly released

oxygen intensifies the reaction with the flammable electrolyte, driving the uncontrollable, self-heating cycle.

5.2.4. Final Events

As internal pressure builds from gas generation and temperature increases (above 300 °C), the cell's safety vent is designed to release the pressure. However, this results in the expulsion of a dark cloud of metal particles and a white vapor cloud containing toxic, flammable gases [126,130]. These gases ignite when exposed to extreme heat or an external spark, creating a high-velocity, jet-like flame that can exceed 600 °C. Along with the flames and intense heat, the TR process releases significant amounts of toxic gases (e.g., CO, CO_2, SO_2, HF, HCl, HCN), organic solvent droplets, and a wide range of short-chain alkanes and alkenes [111,122,133,134]. Among the toxic gases released during TR, carbon monoxide has been identified as one of the primary constituents, with its concentration directly correlated to the SOC of the battery [104,135–137]. Additionally, the cathode chemistry plays a significant role in the amount of CO released. For example, both LCO and NMC batteries release similar levels of CO, while lithium iron phosphate (LFP) batteries emit significantly higher amounts–up to an order of magnitude greater than LCO and NMC batteries [138–140]. If sufficient air is present and the SOC exceeds 50%, this toxic gas vapor typically ignites within one minute, and in confined spaces, it poses serious health risks to anyone exposed. In large battery packs, TR propagates from one cell to adjacent cells in a phenomenon known as cell-to-cell propagation. This occurs when the heat from a cell that has entered TR is transferred to neighboring cells, causing them to overheat and enter TR themselves. This chain reaction can rapidly escalate into a large-scale failure, particularly in tightly packed configurations found in electric vehicle battery packs or energy storage systems.

5.3. Influence of Cell Parameters on Thermal Runaway

The susceptibility of LIBs to TR is strongly influenced by intrinsic parameters like the cell's chemistry, design, and construction. These parameters collectively determine the thermal and electrochemical stability of the battery under TA. Among the key parameters, the electrolyte composition, separator material, electrode materials, SOC, SOH, and overall cell design play a pivotal role in how the cell behaves when subjected to TA [122,141].

5.3.1. Influence of Cell Design

While TR has been extensively studied using various testing methods, there is limited research on how cell design influences this phenomenon. Among the few studies addressing this topic, Lopez et al. [110] investigated the impact of module configuration parameters (such as cell spacing, interconnecting tab style, form factor, and protective materials) on the propagation of TR. They concluded that increasing the distance between cells reduces damage to adjacent cells, raises the overall cell temperature, and minimizes voltage loss. In contrast, a more recent study by Bugryniec et al. [122] focused on the effect of cell geometry on TR by examining gas release in the most commonly used cell types: cylindrical, prismatic, and pouch cells. Their findings indicated that cylindrical cells are less prone to TR compared to prismatic and pouch cells, with a significantly lower total gas release per kilowatt-hour. This discrepancy may also be linked to the aging behavior of LIBs, influenced by the orientation of the cells within the pack [142]. Cylindrical cells are typically arranged vertically, while prismatic and pouch cells can be positioned either flat or vertically inside a pack. Figure 7 shows a comparison of gas release behavior in LCO batteries with different cell geometries during heating at 5 °C/min. Apart from the low SOC condition, the pouch cell produced a higher volume of gas compared with the cylindrical cell.

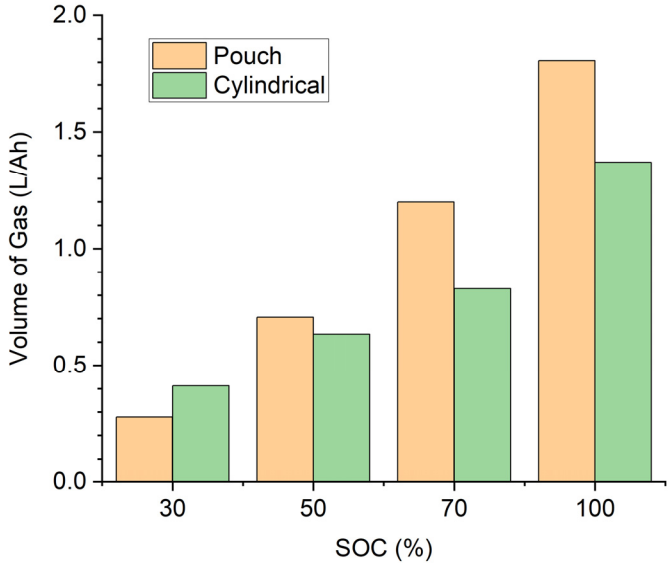

Figure 7. Influence of cell geometry on gas release from LCO batteries heated at 5 °C/min. Data adapted from ref. [143].

The rigid structure and thicker design of prismatic cells hinder heat dissipation, leading to localized hot spots within the cell. Unlike cylindrical cells, which can expand slightly under TA, prismatic cells are more likely to swell or deform due to their lack of flexibility. This can lead to more concentrated heat build-up and an increased risk of failure. In contrast, cylindrical cells have a more uniform heat distribution, which helps maintain a consistent temperature and reduces the likelihood of localized overheating. However, when packed tightly in large battery packs, prismatic cells may experience inefficient heat distribution, which can make certain areas more susceptible to overheating. Pouch cells, though more flexible, tend to have larger surface areas that can aid heat loss to the surrounding environment. However, this is highly dependent on the external cooling and packaging system.

5.3.2. Influence of Cell Composition

Electrolyte Composition

The electrolyte, which consists primarily of lithium salts dissolved in organic solvents, has a significant impact on the thermal stability of the battery. Electrolytes with lower flash points or unstable chemical properties are more prone to decomposition under thermal stress, accelerating the onset of TR. The most commonly used lithium salt, lithium hexafluorophosphate ($LiPF_6$), offers good ionic conductivity, but it decomposes at relatively low temperatures (around 150–200 °C), releasing highly toxic and corrosive by-products such as hydrofluoric acid. These decomposition products not only degrade the battery's internal components but also contribute to a rise in temperature and pressure, fueling TR. Alternatives like lithium tetrafluoroborate ($LiBF_4$) offer better thermal stability but are less conductive and less commercially available, while lithium perchlorate ($LiClO_4$) provides excellent thermal stability but can react explosively under high heat conditions [144].

In addition to the lithium salt, the organic solvents, such as ethylene carbonate, dimethyl carbonate, diethyl carbonate, and ethyl methyl carbonate, also play a crucial role in the thermal response of the battery. Ethylene carbonate has a high melting point and is essential for forming the SEI on the anode, but it undergoes exothermic decomposition at high temperatures, releasing additional heat that accelerates TR [145]. Dimethyl carbonate and diethyl carbonate are less thermally stable and release highly flammable gases like carbon monoxide and carbon dioxide upon decomposition, further contributing

to the thermal escalation. The breakdown of the electrolyte also leads to chemical reactions with the electrode materials, generating more heat and potentially causing internal short circuits [75]. To improve the electrolyte's stability and performance, various additives such as phosphates and borates are often incorporated. These additives help suppress the flammability of the electrolyte solvents and limit the spread of combustion in the event of TA. However, there is often a trade-off between improving safety and maintaining optimal performance, as these additives may influence the overall efficiency of the battery.

Separator Material

The separator in LIBs serves to physically isolate the anode and cathode, preventing direct contact between the electrodes, which could lead to an internal short circuit. It also functions as a thermal fuse or shutdown mechanism, contributing to the battery's structural integrity [146]. The separator material plays a crucial role in determining a lithium-ion battery's response to TA and its overall TR behavior. Key characteristics include melting or softening temperature, shrinkage tendency, mechanical integrity, thermal stability, and shutdown functionality. In applications where safety under abusive or high-stress conditions is paramount, such as electric vehicles, energy storage systems, and aerospace, selecting or engineering separators with superior thermal stability and mechanical robustness is one of the most effective strategies for mitigating the risk of TR.

In portable electronic applications, most lithium-ion batteries typically employ a single polyethylene (PE) separator. In contrast, larger industrial or high-power batteries often use multilayer separators composed of different polymeric materials, such as polypropylene (PP) and polyethylene (PE). The melting point of PE is approximately 135 °C, whereas PP exhibits higher thermal resistance, with a melting point around 165 °C [147–149]. Combining materials with distinct melting points enhances the safety and thermal stability of the separator system.

In multilayer designs (e.g., PP/PE/PP tri-layer separators), the inner PE layer is engineered to melt first, effectively closing the pores and interrupting ion transport, thus shutting down the cell and preventing further current flow. Meanwhile, the outer PP layers remain intact at higher temperatures, maintaining mechanical integrity and providing additional protection. This design offers a "time margin" before catastrophic failure, reducing the likelihood of TR under abusive conditions. The PE layer, therefore, serves as a thermal shutdown component, halting electrochemical reactions during moderate overheating, while the PP layers ensure structural stability until more extreme temperatures are reached. However, if the temperature continues to rise beyond the shutdown threshold, even the PP layers may shrink or fail, potentially leading to internal short circuits [85].

Experimental studies have shown that PP separators can shrink by approximately 50% at around 170 °C, though this thermal shrinkage can be significantly mitigated by applying a ceramic coating. Materials such as Al_2O_3, SiO_2, $Mg(OH)_2$, and TiO_2, often combined with high-temperature-resistant polymers or fibers (e.g., polyimide (PI) or polyether ether ketone (PEEK)), are commonly used for this purpose [85,150]. Such ceramic–polymer composite coatings effectively suppress shrinkage, elevate the thermal failure threshold, and enhance resistance to thermal shorting under abusive operating conditions.

Table 4 summarizes the material properties and thermal-abuse performance of various separators used in lithium-ion batteries. Each separator type exhibits a unique combination of advantages and limitations. Polyethylene is widely used due to its low cost and effective shutdown capability; however, its low melting point leads to rapid shrinkage under high-temperature conditions, increasing the risk of short circuits. Polypropylene provides a higher melting point and better structural integrity at elevated temperatures, but it lacks the thermal-shutdown behavior of PE. Multilayer PP/PE/PP separators combine the benefits

of both polymers, offering a controlled shutdown response from the inner PE layer while maintaining mechanical stability from the outer PP layers.

Table 4. Thermal and safety characteristics of common separator materials used in lithium-ion batteries [85,147–150].

Type	Melting Point (°C)	Shrinkage (%) @150–180 °C	Short-Circuit Risk Under Thermal Abuse
PE (Polyethylene)	130–135	30–60	High if overheating continues
PP (Polypropylene)	160–165	30–50	High above 160 °C
PP/PE/PP Trilayer	130–165	20–40	Moderate if shutdown layer functions
Ceramic-Coated PE/PP (e.g., Al_2O_3, SiO_2, TiO_2 coatings)	130–165	5–15	Low (effective up to 200 °C)
Polyimide	No distinct melting (T_g > 260)	<5	Very Low
PVDF-based Separator	170–180	10–30	Moderate

Ceramic-coated separators exhibit significantly reduced shrinkage and enhanced thermal and mechanical stability, remaining effective up to 200 °C. These are widely adopted in high-safety applications such as electric vehicles. High-performance polymer separators like polyimide (PI) demonstrate excellent thermal resistance and mechanical robustness, showing negligible shrinkage even beyond 260 °C, though their high-cost limits large-scale use. PVDF-based separators provide good chemical and electrochemical stability and moderate thermal tolerance, but are less commonly used as primary separators due to cost and processability considerations.

Electrode Material

Different anode (e.g., graphite, silicon) and cathode (e.g., NMC, LCO) materials significantly influence heat generation behavior under TA conditions. Once the SEI on graphite anodes decomposes, the exposed graphite reacts vigorously with electrolyte solvents. This reaction generates additional heat and flammable gases such as ethylene and hydrogen. However, the anode's contribution to overall heat generation is generally secondary to that of the cathode, since oxygen release from the cathode drives the most critical exothermic reactions.

Layered oxide cathodes, such as LCO and NMC, begin releasing oxygen at elevated temperatures (usually above 180–200 °C) [151]. The liberated oxygen reacts exothermically with the electrolyte and anode materials, accelerating the temperature rise and pressure buildup within the cell. In contrast, LFP cathodes exhibit much higher thermal stability. Their olivine crystal structure effectively suppresses oxygen release, even at temperatures exceeding 250 °C. Consequently, cells employing LFP cathodes typically show a delayed onset of TR and reduced reaction severity compared with those using LCO or NMC [152]. For instance, LFP cathodes at 100% SOC exhibit an onset of heat release between 180 °C and 250 °C, with peak heating occurring between 210 °C and 360 °C [153,154].

5.3.3. Influence of Cell Capacity

The influence of cell capacity on TR triggered by TA is closely linked to the amount of heat generated during operation. Generally, cells with higher capacities produce more heat due to their ability to store and release greater amounts of energy [155]. As a result, large-capacity cells tend to reach the onset of TR more quickly, exhibiting higher peak temperatures, more extensive gas evolution, and more severe venting or rupture compared

to smaller cells. However, the onset temperature of TR is not solely determined by cell capacity. It is also influenced by the internal design and thermal management characteristics of the cell. For example, high-capacity cells often feature thicker electrodes and larger diffusion lengths, which can lead to non-uniform temperature distributions during heating. This localized heating can trigger premature decomposition in certain regions of the cell, accelerating TR. In contrast, smaller-capacity cells typically have better heat dissipation and more uniform internal temperature gradients, delaying the onset of runaway.

Cell capacity also affects the severity of secondary reactions once TR has begun. Larger capacity cells generally experience more pronounced runaway characteristics due to their higher internal heat generation and energy density. These cells tend to exhibit greater temperature rises during TA, resulting in more hazardous thermal events. Furthermore, their larger mass and increased thermal inertia can slow heat dissipation, exacerbating the effects of runaway. While larger capacity cells often have more robust thermal management systems that delay the initiation of TR, once runaway begins, it can be harder to control, leading to more severe consequences. Smaller cells, on the other hand, will heat up and fail more rapidly but typically produce lower amounts of heat and emissions. They are also more likely to self-extinguish shortly after thermal failure, whereas larger cells continue to release energy for a longer duration. The relationship between capacity and TR highlights the importance of understanding how cell size impacts safety across different applications, such as consumer electronics, electric vehicles, and energy storage systems.

5.3.4. Influence of State-of-Charge

The state-of-charge (SOC) refers to the amount of charge relative to a battery's total capacity and is a key factor in both the severity and onset of TR during TA scenarios [139,156]. The relationship between SOC and TR is complex, as it involves several electrochemical, thermal, and structural factors within the battery. When a battery is at a higher SOC, it contains more stored energy, and, as a result, it is more susceptible to TR when exposed to TA and generate significant amounts of heat. This increased energy storage accelerates the onset of TR, making the battery more prone to reaching critical temperatures quickly, leading to more intense TR events [156–158]. Figure 8 presents the results of the Accelerating Rate Calorimetry (ARC) test for NCA-based Li-ion cells, demonstrating that total heat generation increases non-linearly, while the onset temperature of TR decreases with SOC. Consequently, TR parameters, such as the required input thermal energy and the initial temperature necessary to trigger TR, decrease as SOC increases [156,159]. This trend can significantly affect the thermal behavior of adjacent cells within a LIB module [110].

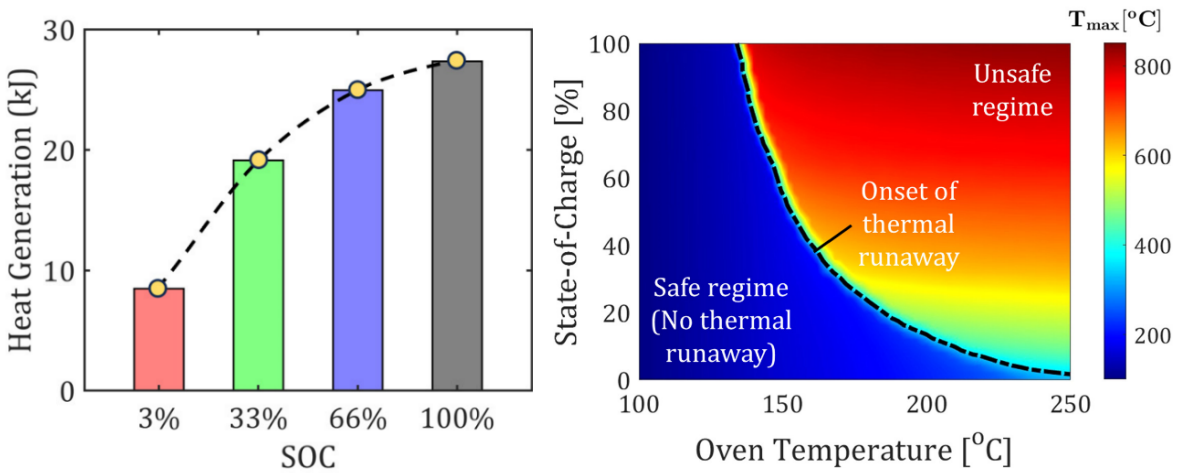

Figure 8. The accelerating rate calorimetry test results of the NCA-based Li-ion cells show the effect of SOC on the total heat generation (left) and onset of thermal runaway (right). Reprinted from [156].

A summary of the venting temperature, TR onset temperature, and maximum temperature at varying SOC levels during TA testing is presented in Table 5. The data indicate that pouch cells exhibit lower venting temperatures, TR onset temperatures, and maximum temperatures compared to cylindrical cells. In contrast, LFP cells display the opposite behavior when compared to NCA and NMC cells, showing higher venting and TR onset temperatures at lower SOCs [160]. However, ARC test data presented by Bugryniec et al. [154] indicate that the venting temperature of LFP cylindrical cells (1500 mAh) is largely independent of the cell's SOC, while the peak temperature increases with higher SOC.

Additionally, the SOC affects the thermal stability of the individual electrode materials [161]. The thermal degradation of key components such as the electrolyte, separator, and electrodes is significantly faster at higher SOCs. This is because the internal voltage is higher, which can lead to faster breakdown of these materials, setting off a chain reaction that leads to TR. Low SOC typically results in lower heat generation during TA, as less energy is stored in the battery. While the likelihood of TR is generally reduced at low SOC, TA can still lead to some damage, such as increased internal resistance and potential failure of the battery's internal components. However, the intensity and speed of TR initiation are less pronounced compared to high SOC conditions.

Table 5. Thermal behavior of cells at varying SOC levels during thermal abuse testing. Data obtained from ref. [162].

Cell Type and Cathode Chemistry	SOC (%)	Venting Temperature (°C)	Thermal Runaway Onset Temperature (°C)	Maximum Temperature (°C)
18650 NCA	100	118	174	710
	50	129	171	649
	40	129	191	482
	30	132	193	468
	15	129	213	427
26650 NMC	100	135	177	522
	50	143	188	628
	40	149	188	581
	30	143	199	557
	15	146	193	409
Pouch NMC	100	77	113	521
	50	81	169	467
	40	88	171	395
	30	93	-	248
	15	96	-	260
Pouch LFP	100	88	132	372
	50	99	154	288
	40	88	157	264
	30	93	-	244
	15	88	-	230

5.4. Temperature Measurement in Thermal Abuse Tests

During TA tests, accurate and precise temperature measurements are critical to fully characterizing the thermal behavior of a battery cell. Monitoring temperature changes at key locations, such as the internal short-circuit region, the cell surface, and near sensitive areas like tabs or electrodes, helps identify the specific conditions that trigger TR. These measurements also provide essential data for modeling the failure process and understand-

ing how cells behave under extreme conditions. Commonly used methods for temperature monitoring include thermocouples, infrared (IR) thermometers, and thermal imaging cameras, each offering unique advantages in terms of spatial resolution, response time, and measurement range [126].

Figure 9 illustrates the voltage and temperature data obtained during a TA test, where a burner was placed beneath the battery module. Both a thermocouple and an IR thermal camera were used to measure the temperature. The area monitored by the IR camera is highlighted in the inset of Figure 9, providing a visual reference for the temperature distribution in the vicinity of the test. As shown in Figure 9, the IR temperature increased sharply immediately after the burner was removed from beneath the module, rising at a rate of approximately 98 °C per second. This rapid temperature increase signaled the onset of TR. The temperature quickly exceeded 600 °C, with the IR camera's calibration ranges spanning 40–150 °C and 100–650 °C. When the temperature exceeded the upper limit of the calibrated range, the IR readings flatlined. Once the temperature dropped back within the camera's measurement range, the device resumed recording, showing a steady decline to approximately 400 °C after about 6 min. This temperature drop coincided with the cessation of visible flames in the monitored area.

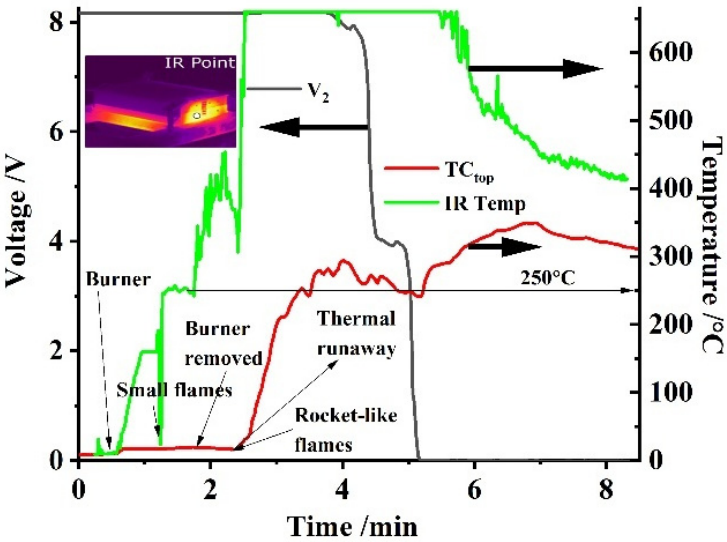

Figure 9. Measured voltage and temperatures during a thermal abuse test of NMC pouch cells. Black arrows indicate the corresponding axis for each curve. Reprinted from [126] with permission from Elsevier.

In contrast, the thermocouple, which measured the surface temperature of the module, exhibited a delayed response of about 2 min compared to the IR readings. Initially, the thermocouple showed little to no increase in temperature until ignition occurred, at which point a flare-like flame emerged. Following ignition, the surface temperature climbed to approximately 275 °C, remaining at this level for about a minute before increasing further to a range of 300–350 °C. These fluctuations in the thermocouple data reflect the unstable nature of the temperature rise, influenced by the dynamic and erratic behavior of the surrounding flames.

The TR temperatures of battery cells are also influenced by the environment in which the tests are conducted. Factors such as ambient temperature, air circulation, and the presence of external heat sources play a crucial role in both the initiation and progression of TR. In controlled laboratory tests, for example, higher ambient temperatures can lower the threshold at which TR occurs, as the cell is already operating closer to its critical temperature range. In contrast, tests conducted at lower ambient temperatures typically show higher

onset temperatures for TR. This is because the cell must generate more internal heat to overcome thermal resistance and reach the critical thresholds required for thermal runaway to initiate. It has been observed that TA tests performed at elevated ambient temperatures result in faster kinetic reactions and a less favorable thermal balance. In these conditions, the cell's ability to dissipate heat is compromised, leading to a rapid accumulation of heat and a much more severe reaction [162–164]. The combination of higher thermal kinetics and poor heat dissipation results in an intensified TR event, underscoring the importance of the environmental conditions in determining the severity of the failure process.

Airflow plays a significant role in shaping the temperature profiles observed during TA tests. Experimental data indicate that the peak temperature during TA is typically lower in open environments compared to tests conducted in semi-confined or enclosed spaces [165]. In environments with restricted airflow, such as enclosed chambers or semi-confined spaces, heat can accumulate around the cell, accelerating the onset of TR. In such conditions, limited ventilation hinders the cell's ability to dissipate the heat generated during failure, leading to a rapid rise in temperature. In contrast, tests conducted in open environments or with forced air circulation allow for more efficient heat dissipation. This can potentially delay the onset of TR or mitigate the severity of the event by reducing the peak temperatures reached. The presence of adequate airflow essentially facilitates heat removal from the battery, helping to prevent the rapid temperature escalation that is characteristic of TR in poorly ventilated spaces.

Additionally, the presence of external heat sources (such as the burner used in Figure 9) alters the thermal behavior of the cell, as the peak temperature during the TA test can be significantly higher than the peak temperature observed during the other abuse tests [128]. This is due to a localized external heat source, which can rapidly raise the temperature of a specific region of the battery, increasing the localized thermal runaway. The intensity, duration, and positioning of such heat sources are important factors in determining the thermal response of the cell. For example, direct application of heat beneath the module, as shown in Figure 9, can cause a rapid temperature rise that mimics or accelerates TR, as seen in the immediate temperature surge and the subsequent heat buildup.

Different battery types and configurations (e.g., cylindrical, prismatic, pouch) exhibit distinct thermal profiles when subjected to TA [166]. For example, cylindrical cells typically show more uniform temperature distributions due to their symmetrical geometry, resulting in relatively lower peak temperatures compared to pouch cells, as shown in Figure 10. In contrast, prismatic and pouch cells, with their unique internal layouts, tend to experience more localized heating, leading to higher temperatures than those observed in cylindrical cells (see Figure 9). Pouch cells, due to their flexible construction, are particularly susceptible to mechanical stresses during TA, a characteristic that distinguishes them from the more rigid structures of prismatic and cylindrical cells. These structural differences not only affect the mechanical stability of the cells but also influence heat generation and dissipation rates. Understanding these design-related thermal behaviors is crucial for accurately assessing battery performance and safety during TA testing.

5.5. Emissions Generated from Thermal Abuse Tests

During the final stage of TR, LIBs release a substantial quantity of gaseous emissions, many of which are toxic and flammable. The vented gases primarily consist of CO and CO_2, which are produced from the combustion and decomposition of the electrolyte and organic binders [104,135–137]. In addition, smaller quantities of hydrogen (H_2), sulfur dioxide (SO_2), nitrogen dioxide (NO_2), hydrogen fluoride (HF), hydrogen chloride (HCl), hydrogen cyanide (HCN), and a variety of short-chain hydrocarbons are typically detected [122,133,134]. These species originate from the breakdown of carbonate-based

electrolytes, the decomposition of the $LiPF_6$ salt, and the combustion of polymeric separator and binder materials.

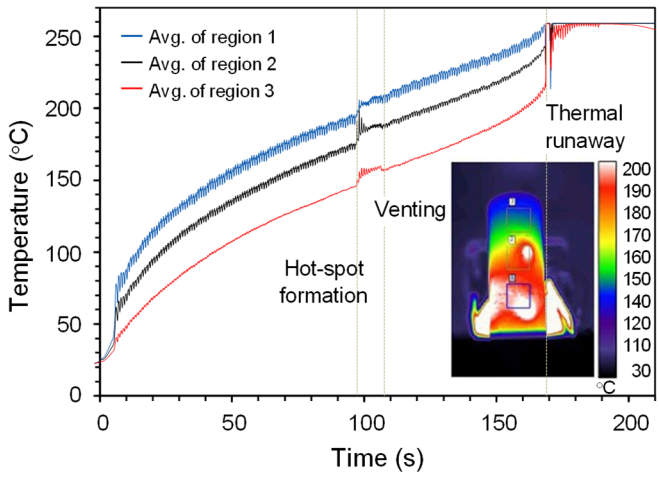

Figure 10. Temperature profile for a cylindrical NMC cell during a thermal abuse test. Reprinted from [166].

The composition and volume of gases generated during TR depend strongly on both the cathode chemistry and the cell design. Figure 11 illustrates that prismatic cells consistently produce the largest volume of gaseous emissions, whereas cylindrical cells generate the least. This difference arises from variations in internal pressure management, electrode surface area, and mechanical containment among cell formats. The flexible pouch-cell design further influences gas release: the laminate casing allows significant expansion during failure, facilitating rapid venting and the escape of toxic vapors.

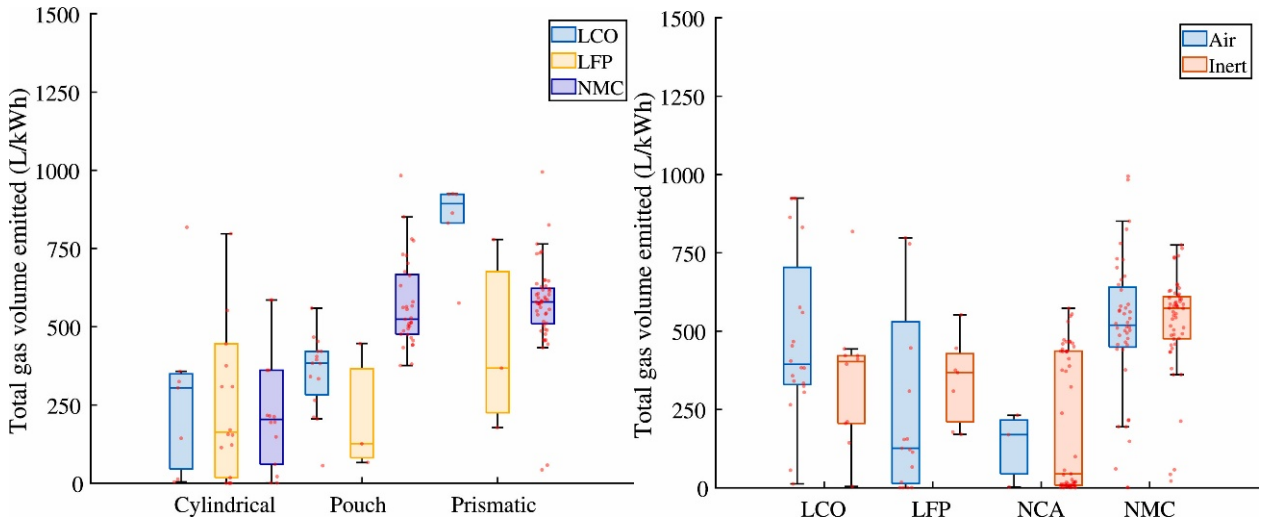

Figure 11. Effect of cell chemistries on the amount of off-gas emitted during LIB failure. Reprinted from [122].

Comparative analysis of different cathode materials shows that LCO and NMC cells emit substantially higher amounts of gas than LFP or NCA cells. This behavior stems from the greater oxygen release and higher reactivity of the transition-metal oxides in LCO and NMC systems, which promote extensive electrolyte oxidation and exothermic decomposition reactions. Conversely, LFP cells are more thermally stable, resulting in reduced gas generation. NMC pouch cells, in particular, tend to emit large quantities

of toxic gases during failure due to accelerated electrolyte breakdown, leading to faster thermal escalation compared with LFP cells.

As shown in Figure 12, real-time monitoring of gas concentrations (CO, CO_2, H_2, and SO_2) during a TA test conducted in a semi-confined environment demonstrates that CO_2 is the dominant emission, followed by CO. The concentrations of H_2 and SO_2 are comparatively minor, though still relevant for safety assessment. The data also indicate that gas generation intensifies with increasing SOC, as higher SOC corresponds to greater stored energy and a more reactive chemical environment. An exception occurs at 25% SOC, where elevated CO_2 levels are observed despite the lower energy content; this is attributed to a slower reaction rate and prolonged combustion, which extends the duration of gas evolution while reducing the overall peak temperature and reaction intensity [165].

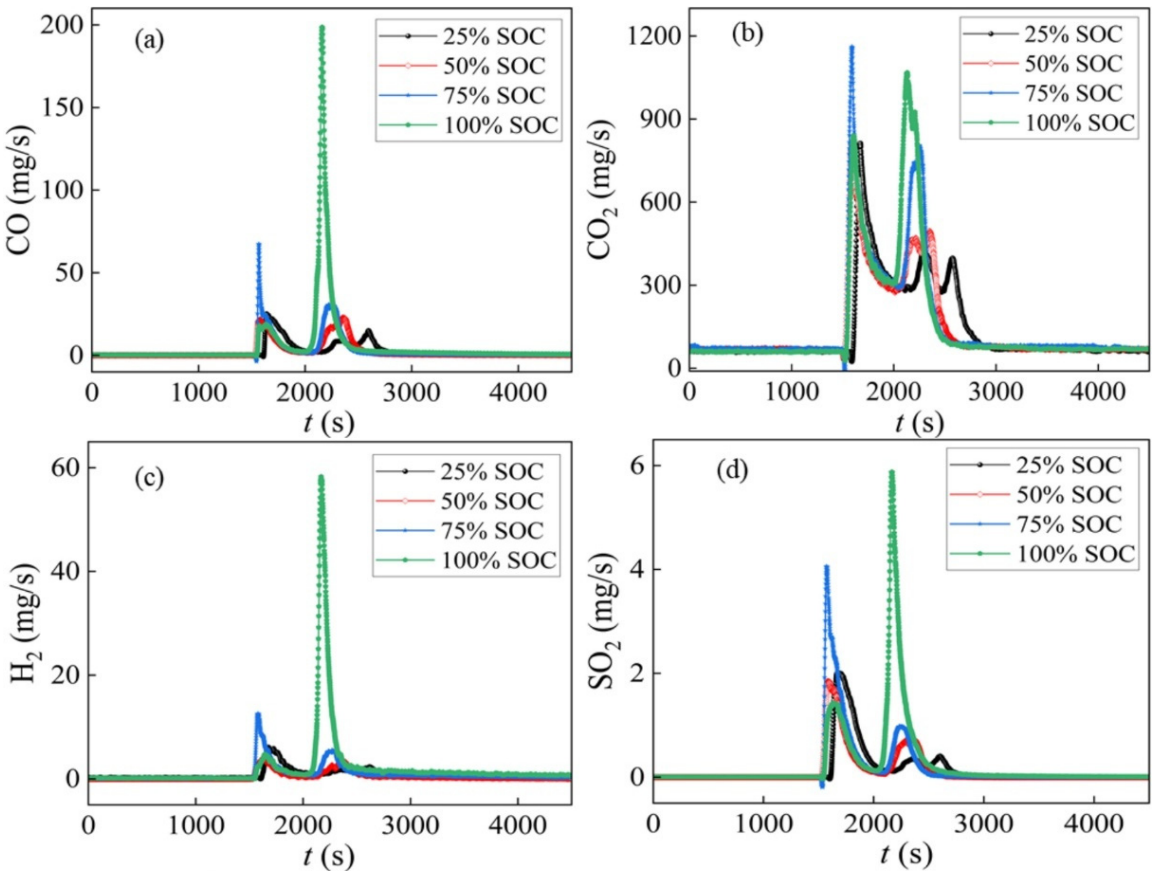

Figure 12. Variations of combustion gases (CO, CO_2, H_2, and SO_2 in parts (**a**), (**b**), (**c**), and (**d**), respectively) during a thermal abuse test in a semi-confined space at different SOCs. Reprinted from [165].

Beyond cell chemistry and geometry, the test environment exerts a strong influence on emission characteristics. Parameters such as ambient temperature, ventilation rate, confinement, and humidity can alter both the composition and the concentration of the released gases and particulates. Elevated ambient temperatures accelerate the decomposition of the electrolyte and electrode materials, thereby enhancing the rate and intensity of toxic gas generation. Conversely, well-ventilated or open test conditions tend to dilute emissions and reduce local concentrations of hazardous species, whereas confined or semi-enclosed environments promote the accumulation of CO, HF, and other noxious gases. Additionally, moisture in the atmosphere can react with fluorinated decomposition products (e.g., PF_5 and POF_3) to form hydrofluoric acid (HF), further increasing the corrosivity and toxicity of the emission plume. Overall, the emission profile during TA is determined by a complex

interplay of electrochemical composition, cell design, and environmental conditions. Understanding these dependencies is essential for developing accurate hazard models and effective mitigation strategies in battery testing and large-scale energy storage applications.

6. Health and Safety Impact of LIB Failures

Studying the health and safety impacts of LIB failures is essential for developing safe systems capable of withstanding the associated risks. As discussed in Section 3, TRs pose a detrimental impact on user safety due to the combined effects of fire, extreme heat, and hazardous emissions [122]. These dangers are further amplified when TR propagates across adjacent cells, modules, or packs, escalating the scale of damage and complicating containment efforts [122].

Fire Hazards: Figure 2c illustrates that fire is the most frequent and immediate hazard during LIB incidents. The rapid release of high-temperature gases under pressure can ignite the TR gases almost instantaneously, forming high-velocity jet flames. Due to concentrated heat flux and directional flame dynamics, such fires can propagate quickly, destroying nearby equipment and materials [167,168]. The intense heat can cause severe cutaneous burns, which may be life-threatening depending on exposure duration and severity [169].

Toxic Emissions: In addition to fire hazards, vented emissions during LIB incidents present significant health risks. Documented incidents, such as the LIB warehouse fire in South Korea, demonstrate that inhalation of toxic smoke alone can be fatal, even before flames spread [170]. These emissions often contain hazardous compounds such as HF, CO, and volatile organic solvents, as shown in Table 6, which can cause respiratory distress, chemical burns, and long-term environmental contamination.

Table 6 summarizes the hazards associated with major emission components identified in LIB failure studies, including their chemical properties, IDLH (Immediately Dangerous to Life or Health) limits, and environmental impacts. These findings underscore the need for robust safety protocols, real-time emission monitoring, and effective firefighting strategies tailored to LIB-specific hazards.

Table 6. Hazards associated with the components found in emissions of LIB incidents.

Emission Component	Chemical Formula	IDLH Levels (ppm or mg/m^3)	Primary Health Effects from Inhalation	Environmental Effects	Reference
Carbon Dioxide	CO_2	40,000 ppm	Headaches, dizziness, difficulty breathing, coma, asphyxia	Greenhouse gas; contributes to global warming and climate change	[171–174]
Carbon Monoxide	CO	1200 ppm	Fatigues, headaches and dizziness	Produces ozone, contributing to climate change	[172,175,176]
Hydrogen	H_2	N/A	No health effects recorded	Releases water vapor, a greenhouse gas	[177,178]
Methane	CH_4	N/A	High concentrations can cause dizziness, vomiting, difficulty breathing, coma, or death	Greenhouse gas, significantly more powerful than CO_2 in trapping heat	[179,180]
Ethylene (ethene)	C_2H_4	N/A	Not harmful to human health at present levels	Not a significant source of environmental pollution	[181]

Table 6. *Cont.*

Emission Component	Chemical Formula	IDLH Levels (ppm or mg/m^3)	Primary Health Effects from Inhalation	Environmental Effects	Reference
Ethane	C_2H_6	N/A	Less toxic at ambient concentrations	Not a significant source of environmental pollution	[182]
Propane	C_3H_8	2100 ppm	High concentrations can displace oxygen, causing headaches, nausea, and dizziness. Less toxic at ambient concentrations.	Not a significant source of environmental pollution	[172,182–184]
Butane	C_4H_{10}	1600 ppm	Less toxic at ambient concentrations.	Not a significant source of environmental pollution	[172,182]
Propylene	C_3H_6	N/A	It can cause frostbite when evaporated. High concentrations of inhalation may lead to depression of the central nervous system.	Not a significant source of environmental pollution at present levels	[185,186]
Hydrofluoric Acid	HF	30 ppm	Eye and respiratory tract irritation at low concentrations, death at high concentrations	Corrodes metals, attacks glass, ceramic, and concrete. Reacts with water and steam creating corrosive fumes	[172,187,188]
Fluoroform (tri-fluoromethane)	CHF_3	N/A	Asphyxiation, dizziness, drowsiness, confusion	Can degrade the ozone layer	[189,190]
Sulfur Dioxide	SO_2	100 ppm	Harmful to respiratory system. Particles may penetrate deeply into the lungs	Contribute to particulate matter (PM) pollution. Decreases growth in trees and plants	[191,192]
Acrolein	C_3H_4O	5 ppm	Eye, nose and throat irritation at 1.22 ppm within 5 s. Other effects include bronchoconstriction and mucus secretion	Classified as a Hazardous Air Pollutant (HAP)	[193–196]
Benzene	C_6H_6	500 ppm	Drowsiness, dizziness headaches, Tremors, death at high exposure levels	Contributes towards smog formation	[172,197,198]
Biphenyl	$C_{12}H_{10}$	100 mg/m^3	Eye and throat irritation, nausea, headache, weakness, liver damage, carcinogen	Classified as a Hazardous Air Pollutant (HAP)	[172,199,200]

Table 6. *Cont.*

Emission Component	Chemical Formula	IDLH Levels (ppm or mg/m^3)	Primary Health Effects from Inhalation	Environmental Effects	Reference
Toluene	C_7H_8	500 ppm	Fatigue, headache, and reduced manual dexterity	Can cause membrane damage in leaves of plants, moderately toxic to aquatic life (acute and chronic). Can breakdown in air to form other harmful chemicals	[172,201,202]
Styrene	C_8H_8	700 ppm	Eye, tract, and skin irritation, nausea, headaches, weakness, possible carcinogen	Toxic to aquatic life, classified as a Hazardous Air Pollutant (HAP)	[172,203]

7. Conclusions and Recommendations

In conclusion, experimental investigations of LIB failures represent a rapidly evolving field, which is driven by the widespread adoption of EVs and the consequent expansion of the LIB market. The rising incidence of LIB-related accidents underscores the urgent need for more rigorous and effective safety assessment methodologies capable of systematically evaluating specific failure outcomes. As outlined in Section 6, LIB emissions can pose severe risks to both human health and the environment, depending on the quantity released and the duration of exposure. Current experimental standards and policies governing LIB safety do not sufficiently encompass the full range of possible failure events and associated risks. Further studies in this area would be highly beneficial in establishing standardized protocols for battery safety. The body of work developed over the past decade provides a critical foundation for such efforts.

As demonstrated throughout Sections 4 and 5, reported outcomes from NP and TA tests exhibit substantial inconsistencies across the literature. For nail penetration, similar cells tested under seemingly comparable conditions led to different outcomes, e.g., full thermal runaway, limited venting, or only swelling, depending on factors such as state of charge, capacity, cathode chemistry, nail characteristics, and test environment. Likewise, thermal abuse studies also report wide variations in TR onset temperature, peak temperature, gas generation, and propagation behavior, because the outcomes can be influenced by heating rate, confinement conditions, and cell geometry. These inconsistencies highlight the strong coupling between intrinsic cell properties and external test parameters, limiting the direct comparability of results across studies.

Current abuse testing standards, including SAE J2464, UL 1642/2580, IEC 62133, and UN 38.3, primarily aim to ensure baseline safety and regulatory compliance rather than to achieve detailed mechanistic understanding or cross-study reproducibility. While these standards provide structured test procedures, they often lack detailed guidance on controlling and reporting parameters critical to failure behavior, such as atmosphere composition, gas collection methodology, heating rate sensitivity, or emission characterization. As a result, variations in experimental implementation can lead to divergent outcomes even when nominally following the same standard.

Future experimental studies would benefit from greater harmonization and transparency in test design and reporting. In particular, explicit reporting of SOC, cell capacity, atmosphere, confinement, and normalization approach is essential for improving comparability. Standardizing key parameters such as penetration speed and incorporating capacity- or energy-normalized emission metrics could reduce variability in reported re-

sults. Additionally, coordinated measurement of thermal, electrical, and emission data would enable clearer separation of TR triggering mechanisms from propagation behavior. Such improvements would enhance the interpretability of abuse test results and support the development of more predictive and application-relevant safety assessments.

While NP tests remain critical for simulating crash-induced failures, TA tests provide insights into heat-driven TR propagation and associated hazards. Both methods reveal that TR severity and emission profiles are strongly influenced by SOC, cell chemistry, and environmental conditions. Regardless of whether it is mechanically or thermally induced, the emissions from LIB failures pose significant health and environmental risks, highlighting the need for standardized testing frameworks that include emission characterization.

Future work should prioritize harmonized protocols for NP and TA tests, integrate real-time emission monitoring, and develop predictive models for TR behavior under diverse abuse scenarios. These steps are essential for improving LIB safety in high-risk applications such as EVs and grid storage. Moving forward, the development of comprehensive testing criteria that address the full spectrum of failure mechanisms associated with TR events will be essential to ensuring reliability, safety, and practical applicability.

Author Contributions: Conceptualization, A.S.N., X.-Y.W., P.K.D. and M.F.; methodology, A.S.N.; formal analysis, A.S.N.; investigation, A.S.N.; data curation, A.S.N.; writing, original draft preparation, A.S.N. (nail penetration section) and P.K.D. (thermal abuse section); writing, review and editing, X.-Y.W., P.K.D. and M.F.; visualization, A.S.N.; supervision, X.-Y.W., P.K.D. and M.F.; funding acquisition, X.-Y.W., P.K.D. and M.F. All authors have read and agreed to the published version of the manuscript.

Funding: XYW acknowledges the funding of the Natural Sciences and Engineering Research Council of Canada (NSERC) [RGPIN-2021–02453]. PKD acknowledges the funding from the Faraday Institution through the ReLiB project, grant numbers FIRG005 and FIRG027. MWF acknowledges the funding by the University of Waterloo, Canada Research Chair Tier I—Zero-Emission Vehicles and Hydrogen Energy Systems, Grant number 950-232215, and the Natural Sciences and Engineering Research Council of Canada (NSERC) Discovery Grants Program [RGPIN-2020-04149].

Data Availability Statement: No new data were created or analyzed in this study. Data sharing is not applicable to this article.

Conflicts of Interest: PKD is a Section Board Member in Batteries and was not involved in the editorial review or the decision to publish this article.

Abbreviations

The following abbreviations are used in this manuscript:

LIB	Lithium-Ion Battery
EV	Electric Vehicle
ZEV	Zero Emission Vehicle
BEV	Battery Electric Vehicle
BESS	Battery Energy Storage System
GHG	Greenhouse Gas
TR	Thermal Runaway
NP	Nail Penetration
TA	Thermal Abuse
SOC	State of Charge
SEI	Solid Electrolyte Interphase
HF	Hydrogen Fluoride (or Hydrofluoric Acid)
CO_2	Carbon Dioxide
CO	Carbon Monoxide
PM	Particulate Matter

PPE	Personal Protective Equipment
UN	United Nations
IEC	International Electrotechnical Commission
UL	Underwriters Laboratories
SAE	Society of Automotive Engineers
CSA	Canadian Standards Association
FTIR	Fourier Transform Infrared Spectroscopy
GC-MS	Gas Chromatography–Mass Spectrometry
QMS	Quadrupole Mass Spectrometry
IC	Ion Chromatography
ARC	Accelerating Rate Calorimetry
NMC	Lithium Nickel Manganese Cobalt Oxide
LFP	Lithium Iron Phosphate
LCO	Lithium Cobalt Oxide
NCA	Lithium Nickel Cobalt Aluminum Oxide
DEC	Diethyl Carbonate
DMC	Dimethyl Carbonate
EMC	Ethyl Methyl Carbonate
EC	Ethylene Carbonate
PP	Polypropylene
PE	Polyethylene
PVDF	Polyvinylidene Fluoride
PI	Polyimide
PEEK	Polyether Ether Ketone

References

1. Environment and Climate Change Canada. Greenhouse Gas Emissions. Available online: https://www.canada.ca/en/environment-climate-change/services/environmental-indicators/greenhouse-gas-emissions.html (accessed on 28 July 2025).
2. Leichter, R. How Much CO_2 Does the Transportation Sector Emit? | Cargoson. Available online: https://www.cargoson.com/en/blog/how-much-co2-does-the-transportation-sector-emit (accessed on 4 December 2025).
3. Transport—Energy System. Available online: https://www.iea.org/energy-system/transport (accessed on 28 July 2025).
4. Demôro, L.; Maia, S.; Aminoff, F. *Energy Transition Factbook*; Bloomberg NEF: London, UK, 2021.
5. Renewables in Transport. Available online: https://www.ren21.net/gsr-2024/ (accessed on 28 July 2025).
6. Viaintermedia. Energy Transition in the Transport Sector Needs to Pick Up Pace, Shows REN21 Report. *Renewable Energy Magazine*. 22 May 2023. Available online: https://www.renewableenergymagazine.com/panorama/energy-transition-in-the-transport-sector-needs-20230522 (accessed on 28 July 2025).
7. Government of Canada. 2030 Emissions Reduction Plan: Clean Air, Strong Economy. Available online: https://www.canada.ca/en/services/environment/weather/climatechange/climate-plan/climate-plan-overview/emissions-reduction-2030.html (accessed on 3 March 2025).
8. IEA. Outlook for Electric Mobility—Global EV Outlook 2024—Analysis. Available online: https://www.iea.org/reports/global-ev-outlook-2024/outlook-for-electric-mobility (accessed on 4 December 2025).
9. Statista. Global EV Market Share. Available online: https://www.statista.com/statistics/1371599/global-ev-market-share/?utm_source=chatgpt.com (accessed on 4 December 2025).
10. Government of Canada. Canada's Zero-Emission Vehicle Sales Targets. Available online: https://tc.canada.ca/en/road-transportation/innovative-technologies/zero-emission-vehicles/canada-s-zero-emission-vehicle-sales-targets (accessed on 12 June 2025).
11. Jarratt, E. ZEVs Leap to 16.5 Percent Market Share in Q3 2024: S&P Global. Available online: https://electricautonomy.ca/data-trackers/2024-11-23/sp-q3-2024-zev-registration-canada/ (accessed on 23 November 2024).
12. Fan, Y.; Wang, Z.; Xiong, X.; Panchal, S.; Fraser, R.; Fowler, M. Multi-Objective Optimization Design and Experimental Investigation for a Prismatic Lithium-Ion Battery Integrated with a Multi-Stage Tesla Valve-Based Cold Plate. *Processes* **2023**, *11*, 1618. [CrossRef]
13. Zubi, G.; Dufo-López, R.; Carvalho, M.; Pasaoglu, G. The lithium-ion battery: State of the art and future perspectives. *Renew. Sustain. Energy Rev.* **2018**, *89*, 292–308. [CrossRef]

14. Battery University. BU-107: Comparison Table of Secondary Batteries. Available online: https://batteryuniversity.com/article/bu-107-comparison-table-of-secondary-batteries (accessed on 28 July 2025).
15. Government of Canada. Battery Safety: Lithium-Ion Batteries. Available online: https://www.canada.ca/en/health-canada/services/household-products/battery-safety/lithium-ion.html (accessed on 13 July 2025).
16. US Department of Energy. Batteries for Electric Vehicles: Alternatives Fuels Data Center. Available online: https://afdc.energy.gov/vehicles/electric-batteries (accessed on 20 February 2025).
17. Michael Franklin Calgary Fire Department Launches Lithium-Ion Battery Safety Campaign. *CTV News*. 6 November 2024. Available online: https://www.ctvnews.ca/calgary/article/calgary-fire-department-launches-lithium-ion-battery-safety-campaign/ (accessed on 20 February 2025).
18. Ahmed, M.; Mao, Z.; Liu, Y.; Yu, A.; Fowler, M.; Chen, Z. Comparative Analysis of Computational Times of Lithium-Ion Battery Management Solvers and Battery Models Under Different Programming Languages and Computing Architectures. *Batteries* **2024**, *10*, 439. [CrossRef]
19. IEA. Trends in Electric Vehicle Batteries—Global EV Outlook 2024—Analysis. Available online: https://www.iea.org/reports/global-ev-outlook-2024/trends-in-electric-vehicle-batteries (accessed on 28 July 2025).
20. Global EV Outlook 2024. International Energy Agency. 2024. Available online: https://www.iea.org/reports/global-ev-outlook-2024 (accessed on 11 February 2025).
21. Zablocki, A. Fact Sheet | Energy Storage. 22 February 2019. Available online: https://www.eesi.org/papers/view/energy-storage-2019 (accessed on 23 February 2025).
22. Tao, C.; Li, G.; Zhao, J.; Chen, G.; Wang, Z.; Qian, Y.; Cheng, X.; Liu, X. The investigation of thermal runaway propagation of lithium-ion batteries under different vertical distances. *J. Therm. Anal. Calorim.* **2020**, *142*, 1523–1532. [CrossRef]
23. Sharma, H.; Sharma, S.; Mishra, P.K. A critical review of recent progress on lithium ion batteries: Challenges, applications, and future prospects. *Microchem. J.* **2025**, *212*, 113494. [CrossRef]
24. Khalid, R.; Shah, A.; Javed, M.; Hussain, H. Progress and obstacles in electrode materials for lithium-ion batteries: A journey towards enhanced energy storage efficiency. *RSC Adv.* **2025**, *15*, 15951–15998. [CrossRef]
25. Yao, L.; Yu, C.; Xiao, Y.; Cui, G.; Fei, Z.; Qu, C. A comprehensive review of lithium-ion battery safety issues and fault diagnosis strategies throughout the entire lifecycle. *J. Energy Storage* **2025**, *136*, 118447. [CrossRef]
26. Zanoletti, A.; Carena, E.; Ferrara, C.; Bontempi, E. A Review of Lithium-Ion Battery Recycling: Technologies, Sustainability, and Open Issues. *Batteries* **2024**, *10*, 38. [CrossRef]
27. Madani, S.S.; Shabeer, Y.; Nair, A.S.; Fowler, M.; Panchal, S.; Ziebert, C.; Chaoui, H.; Dou, S.X.; See, K.; Mekhilef, S.; et al. Advances in Battery Modeling and Management Systems: A Comprehensive Review of Techniques, Challenges, and Future Perspectives. *Batteries* **2025**, *11*, 426. [CrossRef]
28. Nishi, Y. The Dawn of Lithium-Ion Batteries. *Electrochem. Soc. Interface* **2016**, *25*, 71–74. [CrossRef]
29. Le, A.; Wang, M.; Shi, Y.; Noelle, D.; Qiao, Y. Heat generation of mechanically abused lithium-ion batteries modified by carbon black micro-particulates. *J. Phys. Appl. Phys.* **2015**, *48*, 385501. [CrossRef]
30. Pan, Z.; Li, W.; Xia, Y. Experiments and 3D detailed modeling for a pouch battery cell under impact loading. *J. Energy Storage* **2020**, *27*, 101016. [CrossRef]
31. Wierzbicki, T.; Sahraei, E. Homogenized mechanical properties for the jellyroll of cylindrical Lithium-ion cells. *J. Power Sources* **2013**, *241*, 467–476. [CrossRef]
32. Giffin, G.A. The role of concentration in electrolyte solutions for non-aqueous lithium-based batteries. *Nat. Commun.* **2022**, *13*, 5250. [CrossRef]
33. Koech, A.K.; Mwandila, G.; Mulolani, F.; Mwaanga, P. Lithium-ion battery fundamentals and exploration of cathode materials: A review. *S. Afr. J. Chem. Eng.* **2024**, *50*, 321–339. [CrossRef]
34. Lain, M.J.; Kendrick, E. Understanding the limitations of lithium ion batteries at high rates. *J. Power Sources* **2021**, *493*, 229690. [CrossRef]
35. Ouyang, D.; Chen, M.; Liu, J.; Wei, R.; Weng, J.; Wang, J. Investigation of a commercial lithium-ion battery under overcharge/over-discharge failure conditions. *RSC Adv.* **2018**, *8*, 33414–33424. [CrossRef]
36. Luiso, S.; Fedkiw, P. Lithium-ion battery separators: Recent developments and state of art. *Curr. Opin. Electrochem.* **2020**, *20*, 99–107. [CrossRef]
37. Cherkashinin, G.; Hausbrand, R.; Jaegermann, W. Performance of Li-Ion Batteries: Contribution of Electronic Factors to the Battery Voltage. *J. Electrochem. Soc.* **2019**, *166*, A5308. [CrossRef]
38. Okubo, M.; Ko, S.; Dwibedi, D.; Yamada, A. Designing positive electrodes with high energy density for lithium-ion batteries. *J. Mater. Chem. A* **2021**, *9*, 7407–7421. [CrossRef]
39. Kwon, S.-J.; Lee, S.-E.; Lim, J.-H.; Choi, J.; Kim, J. Performance and Life Degradation Characteristics Analysis of NCM LIB for BESS. *Electronics* **2018**, *7*, 406. [CrossRef]

40. Jyoti, J.; Singh, B.P.; Tripathi, S.K. Recent advancements in development of different cathode materials for rechargeable lithium ion batteries. *J. Energy Storage* **2021**, *43*, 103112. [CrossRef]
41. Tran, M.-K.; DaCosta, A.; Mevawalla, A.; Panchal, S.; Fowler, M. Comparative Study of Equivalent Circuit Models Performance in Four Common Lithium-Ion Batteries: LFP, NMC, LMO, NCA. *Batteries* **2021**, *7*, 51. [CrossRef]
42. Venegas, N. 3 Dead After Tesla Cybertruck Crashes and Catches Fire. *Newsweek*. 27 November 2024. Available online: https://www.newsweek.com/3-dead-after-tesla-cybertruck-crashes-catches-fire-1992789 (accessed on 3 March 2025).
43. Quraishi, A.; Novak, A. Lithium Battery Fires on U.S. Flights Now Occur Nearly Twice a Week, According to New FAA Data. *CBS News*. 18 December 2024. Available online: https://www.cbsnews.com/news/lithium-battery-fires-us-flights-new-faa-data/ (accessed on 6 March 2025).
44. 4 killed in fiery electric vehicle crash in downtown Toronto. *CBC News*. 24 October 2024. Available online: https://www.cbc.ca/news/canada/toronto/fatal-crash-four-dead-lake-shore-cherry-1.7361751 (accessed on 6 March 2025).
45. UL Solutions. Lithium-ion Battery Incident Reporting. Available online: https://www.ul.com/insights/lithium-ion-battery-incident-reporting (accessed on 15 April 2025).
46. Damaged batteries should stay dead"—Calgary Fire Department launches awareness campaign about lithium-ion battery safety. *The City of Calgary Newsroom*. 6 November 2024. Available online: https://newsroom.calgary.ca/damaged-batteries-should-stay-dead--calgary-fire-department-launches-awareness-campaign-about-lithium-ion-battery-safety/ (accessed on 14 March 2025).
47. Fernandez, M. Lithium-ion battery fires jump 162% in Toronto over 2 years, city says. *CBC News*. 7 July 2025. Available online: https://www.cbc.ca/news/canada/toronto/toronto-lithium-ion-battery-fires-1.7578827 (accessed on 4 December 2025).
48. Alyse Kotyk Report reveals leading cause of Vancouver fires in 2023. *CTV News*. 6 March 2024. Available online: https://www.ctvnews.ca/vancouver/article/report-reveals-leading-cause-of-vancouver-fires-in-2023/ (accessed on 18 March 2025).
49. Isaac Olson A lithium battery fire sent toxic gas over Montreal. Are we ready for such emergencies? *CBC News*. 28 September 2024. Available online: https://www.cbc.ca/news/canada/montreal/montreal-lithium-battery-fire-concerns-1.7336652 (accessed on 18 March 2025).
50. Villalovas, E. NYC E-Bike Battery Deaths and Injuries Hit Record High in 2023. Available online: https://www.washingtonexaminer.com/policy/infrastructure/2805999/e-bike-battery-fire-deaths-rise-new-york-city/ (accessed on 4 December 2025).
51. Toombs, A. Calgary Fire Department urges caution with lithium-ion batteries ahead of holiday season. *LiveWire Calgary*. 6 November 2024. Available online: https://livewirecalgary.com/2024/11/06/calgary-fire-department-urges-caution-with-lithium-ion-batteries-ahead-of-holiday-season/ (accessed on 30 March 2025).
52. Bryan Bicknell Fire officials raise concerns over EV fires. *CTV News*. 19 December 2023. Available online: https://www.ctvnews.ca/london/article/fire-officials-raise-concerns-over-ev-fires/ (accessed on 2 April 2025).
53. Liu, J.; Xu, N.; Shi, Y.; Barnett, T.; Jones, S. Are first responders prepared for electric vehicle fires? A national survey. *Accid. Anal. Prev.* **2023**, *179*, 106903. [CrossRef]
54. Jonathan Migneault Electric vehicle battery fires remain poorly understood as mining industry transitions to the technology. *CBC News*. 16 February 2024. Available online: https://www.cbc.ca/news/canada/sudbury/electric-battery-fires-mining-1.7117483 (accessed on 2 April 2025).
55. Dodds, J. New NFPA research project investigates lithium-ion battery fires' impact on firefighters, PPE. *Fire Fighting in Canada*. 20 December 2024. Available online: https://www.firefightingincanada.com/new-nfpa-research-project-investigates-lithium-ion-battery-fires-impact-on-firefighters-ppe/ (accessed on 6 April 2025).
56. Transport Canada. Transporting Batteries. Available online: https://tc.canada.ca/en/dangerous-goods/transporting-batteries (accessed on 19 April 2025).
57. Special Provisions. Available online: https://laws-lois.justice.gc.ca/eng/regulations/SOR-2001-286/page-32.html#h-1230891 (accessed on 19 April 2025).
58. United Nations. Section 38.3, Recommendations on the Transport of Dangerous Goods. In *Manual of Tests and Criteria*; United Nations: New York, NY, USA, 2019.
59. PART 2 Classification (Continued) Class 6, Toxic and Infectious Substances (Continued). Available online: https://laws-lois.justice.gc.ca/eng/regulations/sor-2001-286/page-10.html#h-1228702 (accessed on 19 April 2025).
60. Transport Canada. Lithium Batteries. Available online: https://tc.canada.ca/en/lithium-batteries (accessed on 19 April 2025).
61. Transport Canada. Research Summary—Evaluation and Analysis of Substandard Lithium-Ion Batteries by UN 38.3 Testing. Available online: https://tc.canada.ca/en/dangerous-goods/publications/lithium-battery-transport-research/research-summary-evaluation-analysis-substandard-lithium-ion-batteries-383-testing (accessed on 19 April 2025).
62. Intertek. UN 38.3 Testing for Lithium Batteries. Available online: https://www.intertek.com/batteries/un-38-3-testing/ (accessed on 19 April 2025).

63. Sun, Y.; Yuan, Y.; Lu, L.; Han, X.; Kong, X.; Wang, H.; Ouyang, M.; Gao, P.; Zheng, H.; Wang, K. A comprehensive research on internal short circuits caused by copper particle contaminants on cathode in lithium-ion batteries. *eTransportation* **2022**, *13*, 100183. [CrossRef]
64. Aalund, R.; Pecht, M. The Use of UL 1642 Impact Testing for Li-ion Pouch Cells. *IEEE Access* **2019**, *7*, 176706–176711. [CrossRef]
65. Fonseca, E.; Franco, R.A.; Simons, B.; Paiss, D.M. Challenges in Deploying a Second-Life Battery System: Engineering, Fire Safety, UL Certifications, and NFPA Requirements. In *Proceedings of the 2024 IEEE Electrical Energy Storage Application and Technologies Conference (EESAT), San Diego, CA, USA, 29–30 January 2024*; IEEE: Piscataway, NJ, USA, 2024; pp. 1–5.
66. *IEC 62133-2 2017*; Secondary Cells and Batteries Containing Alkaline or Other Non-Acid Electrolytes—Safety Requirements for Portable Sealed Secondary Cells, and for Batteries Made from Them, for Use in Portable Applications—Part 2: Lithium Systems. International Electrotechnical Commission: Geneva, Switzerland, 2017. Available online: https://webstore.iec.ch/en/publication/32662 (accessed on 19 April 2025).
67. Chen, Y.; Kang, Y.; Zhao, Y.; Wang, L.; Liu, J.; Li, Y.; Liang, Z.; He, X.; Li, X.; Tavajohi, N.; et al. A review of lithium-ion battery safety concerns: The issues, strategies, and testing standards. *J. Energy Chem.* **2021**, *59*, 83–99. [CrossRef]
68. *J2464_202108*; Electric and Hybrid Electric Vehicle Rechargeable Energy Storage System (RESS) Safety and Abuse Testing. SAE International: Washington, DC, USA, 2021. Available online: https://www.sae.org/standards/content/j2464_202108/ (accessed on 15 April 2025).
69. *SAE J2464*; Testing for Rechargeable Energy Storage Systems. Southwest Research Institute: San Antonio, TX, USA, 2009. Available online: https://www.swri.org/markets/automotive-transportation/automotive/battery-testing-research/sae-j2464-testing-rechargeable-energy-storage-systems (accessed on 4 December 2025).
70. Lai, X.; Yao, J.; Jin, C.; Feng, X.; Wang, H.; Xu, C.; Zheng, Y. A Review of Lithium-Ion Battery Failure Hazards: Test Standards, Accident Analysis, and Safety Suggestions. *Batteries* **2022**, *8*, 248. [CrossRef]
71. Ma, S.; Jiang, M.; Tao, P.; Song, C.; Wu, J.; Wang, J.; Deng, T.; Shang, W. Temperature effect and thermal impact in lithium-ion batteries: A review. *Prog. Nat. Sci. Mater. Int.* **2018**, *28*, 653–666. [CrossRef]
72. Himaxbattery. Charging Lithium Batteries: Temperature, Safety & Best Practices. Available online: https://www.himaxbattery.com/2025/10/22/charging-lithium-batteries-at-high-and-low-temperatures-a-practical-guide-for-buyers-and-designers/ (accessed on 4 December 2025).
73. Gupta, V.; Dunn, M.J.; Macfarlane, A.R.W.; Xiao, T.; Farooq, A.; Masri, A.R. Analysis of ejecta ignition and velocity from 18650 Li-ion battery cells during thermal runaway. *J. Power Sources* **2025**, *653*, 237697. [CrossRef]
74. Tomaszewska, A.; Chu, Z.; Feng, X.; O'Kane, S.; Liu, X.; Chen, J.; Ji, C.; Endler, E.; Li, R.; Liu, L.; et al. Lithium-ion battery fast charging: A review. *eTransportation* **2019**, *1*, 100011. [CrossRef]
75. Dai, Y.; Panahi, A. Thermal runaway process in lithium-ion batteries: A review. *Energy* **2025**, *6*, 100186. [CrossRef]
76. Sun, W.; Yang, B.; Hansen, N.; Westbrook, C.K.; Zhang, F.; Wang, G.; Moshammer, K.; Law, C.K. An experimental and kinetic modeling study on dimethyl carbonate (DMC) pyrolysis and combustion. *Combust. Flame* **2016**, *164*, 224–238. [CrossRef]
77. Kanayama, K.; Takahashi, S.; Nakamura, H.; Tezuka, T.; Maruta, K. Experimental and modeling study on pyrolysis of ethylene carbonate/dimethyl carbonate mixture. *Combust. Flame* **2022**, *245*, 112359. [CrossRef]
78. Takahashi, S.; Kanayama, K.; Morikura, S.; Nakamura, H.; Tezuka, T.; Maruta, K. Study on oxidation and pyrolysis of carbonate esters using a micro flow reactor with a controlled temperature profile. Part II: Chemical kinetic modeling of ethyl methyl carbonate. *Combust. Flame* **2022**, *238*, 111878. [CrossRef]
79. Sun, W.; Huang, C.; Tao, T.; Zhang, F.; Li, W.; Hansen, N.; Yang, B. Exploring the high-temperature kinetics of diethyl carbonate (DEC) under pyrolysis and flame conditions. *Combust. Flame* **2017**, *181*, 71–81. [CrossRef]
80. Sadeghi, H.; Restuccia, F. Kinetic modelling of thermal decomposition in lithium-ion battery components during thermal runaway. *J. Power Sources* **2025**, *629*, 236026. [CrossRef]
81. Premnath, V.; Wang, Y.; Wright, N.; Khalek, I.; Uribe, S. Detailed characterization of particle emissions from battery fires. *Aerosol Sci. Technol.* **2022**, *56*, 337–354. [CrossRef]
82. Mao, Y.; Chen, Y.; Chen, M. Review of Flame Behavior and Its Suppression during Thermal Runaway in Lithium-Ion Batteries. *Batteries* **2024**, *10*, 307. [CrossRef]
83. Yang, Y.; Wang, R.; Shen, Z.; Yu, Q.; Xiong, R.; Shen, W. Towards a safer lithium-ion batteries: A critical review on cause, characteristics, warning and disposal strategy for thermal runaway. *Adv. Appl. Energy* **2023**, *11*, 100146. [CrossRef]
84. Lin, L.S.; Li, J.L.; Fishman, I.M.; Torres-Castro, L.; Preger, Y.; De Angelis, V.; Lamb, J.; Zhu, X.Q.; Allu, S.; Wang, H. Mechanically induced thermal runaway severity analysis for Li-ion batteries. *J. Energy Storage* **2023**, *61*, 106798. [CrossRef]
85. Tong, B.; Li, X. Towards separator safety of lithium-ion batteries: A review. *Mater. Chem. Front.* **2024**, *8*, 309–340. [CrossRef]
86. Feng, L.; Jiang, L.; Liu, J.; Wang, Z.; Wei, Z.; Wang, Q. Dynamic overcharge investigations of lithium ion batteries with different state of health. *J. Power Sources* **2021**, *507*, 230262. [CrossRef]
87. Das, S.; Shrotriya, P. Electrochemical Mechanism Underlying Lithium Plating in Batteries: Non-Invasive Detection and Mitigation. *Energies* **2024**, *17*, 5930. [CrossRef]

88. Sabeel, K.; Al-Greer, M.; Bashir, I. Advancements in Vibration Testing: Effects on Thermal Performance and Degradation of Modern Batteries. *Batteries* **2025**, *11*, 82. [CrossRef]
89. Fink, K.E.; Polzin, B.J.; Vaughey, J.T.; Major, J.J.; Dunlop, A.R.; Trask, S.E.; Jeka, G.T.; Spangenberger, J.S.; Keyser, M.A. Influence of metallic contaminants on the electrochemical and thermal behavior of Li-ion electrodes. *J. Power Sources* **2022**, *518*, 230760. [CrossRef]
90. National Research Council Canada. NRC Lithium-Ion Battery Safety Test Sparks International Acclaim. Available online: https://nrc.canada.ca/en/stories/nrc-lithium-ion-battery-safety-test-sparks-international-acclaim (accessed on 25 July 2025).
91. Winter, M.; Barnett, B.; Xu, K. Before Li Ion Batteries. *Chem. Rev.* **2018**, *118*, 11433–11456. [CrossRef]
92. Ouyang, D.; Chen, M.; Huang, Q.; Weng, J.; Wang, Z.; Wang, J. A Review on the Thermal Hazards of the Lithium-Ion Battery and the Corresponding Countermeasures. *Appl. Sci.* **2019**, *9*, 2483. [CrossRef]
93. Emmet, H. Updates to Lithium Ion Thermal Runaway Reduction Act. Available online: https://hct-world.com/thermal-runaway-reduction-act/ (accessed on 25 July 2025).
94. Federal Register. Federal Motor Vehicle Safety Standards; FMVSS No. 305a Electric-Powered Vehicles: Electric Powertrain Integrity Global Technical Regulation No. 20 Incorporation by Reference. Available online: https://www.federalregister.gov/documents/2024/12/20/2024-28707/federal-motor-vehicle-safety-standards-fmvss-no-305a-electric-powered-vehicles-electric-powertrain (accessed on 25 July 2025).
95. Saxena, S.; Pecht, M. Accelerated Life Testing of Lithium-ion Batteries. Available online: https://www.batterypoweronline.com/news/accelerated-life-testing-of-lithium-ion-batteries/# (accessed on 14 December 2024).
96. Kelleher, S.R. Lithium Battery Fire Forced Emergency Flight Landing Last Weekend—Following A String of Similar Incidents. Available online: https://www.forbes.com/sites/suzannerowankelleher/2025/08/26/lithium-battery-fires-planes-concerns-aviation-pros/ (accessed on 5 September 2025).
97. Warning After Homemade e-Bike Battery Sparks Peterborough Fire. Available online: https://www.bbc.com/news/articles/cy9nejnz7plo (accessed on 5 September 2025).
98. Diao, W.; Saxena, S.; Pecht, M. Accelerated cycle life testing and capacity degradation modeling of LiCoO2-graphite cells. *J. Power Sources* **2019**, *435*, 226830. [CrossRef]
99. Zhao, J.; Feng, X.; Tran, M.-K.; Fowler, M.; Ouyang, M.; Burke, A.F. Battery safety: Fault diagnosis from laboratory to real world. *J. Power Sources* **2024**, *598*, 234111. [CrossRef]
100. Zhang, L.; Liu, Y.; Huang, X. Dynamic thermal runaway evolution of Li-ion battery during nail penetration. *Int. J. Heat Mass Transf.* **2024**, *233*, 126020. [CrossRef]
101. Essl, C.; Golubkov, A.W.; Fuchs, A. Comparing Different Thermal Runaway Triggers for Two Automotive Lithium-Ion Battery Cell Types. *J. Electrochem. Soc.* **2020**, *167*, 130542. [CrossRef]
102. Koch, S.; Birke, K.P.; Kuhn, R. Fast Thermal Runaway Detection for Lithium-Ion Cells in Large Scale Traction Batteries. *Batteries* **2018**, *4*, 16. [CrossRef]
103. Doose, S.; Haselrieder, W.; Kwade, A. Effects of the Nail Geometry and Humidity on the Nail Penetration of High-Energy Density Lithium Ion Batteries. *Batteries* **2021**, *7*, 6. [CrossRef]
104. Nedjalkov, A.; Meyer, J.; Köhring, M.; Doering, A.; Angelmahr, M.; Dahle, S.; Sander, A.; Fischer, A.; Schade, W. Toxic Gas Emissions from Damaged Lithium Ion Batteries—Analysis and Safety Enhancement Solution. *Batteries* **2016**, *2*, 5. [CrossRef]
105. Willstrand, O.; Pushp, M.; Andersson, P.; Brandell, D. Impact of different Li-ion cell test conditions on thermal runaway characteristics and gas release measurements. *J. Energy Storage* **2023**, *68*, 107785. [CrossRef]
106. Buston, J.E.H.; Gill, J.; Lisseman, R.; Morton, J.; Musgrove, D.; Williams, R.C.E. Experimental determination of metals generated during the thermal failure of lithium ion batteries. *Energy Adv.* **2023**, *2*, 170–179. [CrossRef]
107. Ghiji, M.; Edmonds, S.; Moinuddin, K. A Review of Experimental and Numerical Studies of Lithium Ion Battery Fires. *Appl. Sci.* **2021**, *11*, 1247. [CrossRef]
108. Abaza, A.; Ferrari, S.; Wong, H.K.; Lyness, C.; Moore, A.; Weaving, J.; Blanco-Martin, M.; Dashwood, R.; Bhagat, R. Experimental study of internal and external short circuits of commercial automotive pouch lithium-ion cells. *J. Energy Storage* **2018**, *16*, 211–217. [CrossRef]
109. Spotnitz, R.; Franklin, J. Abuse behavior of high-power, lithium-ion cells. *J. Power Sources* **2003**, *113*, 81–100. [CrossRef]
110. Lopez, C.F.; Jeevarajan, J.A.; Mukherjee, P.P. Experimental Analysis of Thermal Runaway and Propagation in Lithium-Ion Battery Modules. *J. Electrochem. Soc.* **2015**, *162*, A1905. [CrossRef]
111. Sun, P.; Bisschop, R.; Niu, H.; Huang, X. A Review of Battery Fires in Electric Vehicles. *Fire Technol.* **2020**, *56*, 1361–1410. [CrossRef]
112. Lamb, J.; Orendorff, C.; Roth, E.; Langendorf, J. Studies on the Thermal Breakdown of Common Li-Ion Battery Electrolyte Components. *J. Electrochem. Soc.* **2015**, *162*, A2131–A2135. [CrossRef]
113. Diaz, F.; Wang, Y.; Weyhe, R.; Friedrich, B. Gas generation measurement and evaluation during mechanical processing and thermal treatment of spent Li-ion batteries. *Waste Manag.* **2019**, *84*, 102–111. [CrossRef]

114. Hoelle, S.; Scharner, S.; Asanin, S.; Hinrichsen, O. Analysis on Thermal Runaway Behavior of Prismatic Lithium-Ion Batteries with Autoclave Calorimetry. *J. Electrochem. Soc.* **2021**, *168*, 120515. [CrossRef]
115. Diekmann, J.; Doose, S.; Weber, S.; Münch, S.; Haselrieder, W.; Kwade, A. Development of a New Procedure for Nail Penetration of Lithium-Ion Cells to Obtain Meaningful and Reproducible Results. *J. Electrochem. Soc.* **2020**, *167*, 090504. [CrossRef]
116. Howard, G.E.; Buston, J.E.H.; Gill, J.; Goddard, S.L.; Mellor, J.W.; Reeve, P.A.P. Comprehensive Study of the Gas Volume and Composition Produced by Different 3–230 Ah Lithium Iron Phosphate (LFP) Cells Failed Using External Heat, Overcharge and Nail Penetration Under Air and Inert Atmospheres. *Batteries* **2025**, *11*, 267. [CrossRef]
117. Comprehensive Study of the Gas Volume and Composition Generated by 5 Ah Nickel Manganese Cobalt Oxide (NMC) Li-Ion Pouch Cells Through Different Failure Mechanisms at Varying States of Charge. Available online: https://www.mdpi.com/2313-0105/11/5/197 (accessed on 24 July 2025).
118. Reeve, P.A.P.; Buston, J.E.H.; Gill, J.; Goddard, S.L.; Howard, G.E.; Mellor, J.W. Failure gas analysis of lithium–nickel–cobalt–aluminium oxide cells from different manufacturers. *RSC Adv.* **2025**, *15*, 5084–5095. [CrossRef]
119. Walker, W.Q.; Bayles, G.A.; Johnson, K.L.; Brown, R.P.; Petrushenko, D.; Hughes, P.J.; Calderon, D.T.; Darst, J.J.; Hagen, R.A.; Sakowski, B.A.; et al. Evaluation of Large-Format Lithium-Ion Cell Thermal Runaway Response Triggered by Nail Penetration using Novel Fractional Thermal Runaway Calorimetry and Gas Collection Methodology. *J. Electrochem. Soc.* **2022**, *169*, 060535. [CrossRef]
120. The Effects of Cell Chemistry, State of Charge, and Abuse Method on Gas Generation in Li-ion Cell Failure. Available online: https://www.mdpi.com/2313-0105/11/9/320 (accessed on 3 September 2025).
121. Thermocouple Types—Types of thermocouples—Comparison of Thermocouple Types. Available online: https://www.thermocoupleinfo.com/thermocouple-types.htm (accessed on 4 September 2025).
122. Bugryniec, P.J.; Resendiz, E.G.; Nwophoke, S.M.; Khanna, S.; James, C.; Brown, S.F. Review of gas emissions from lithium-ion battery thermal runaway failure—Considering toxic and flammable compounds. *J. Energy Storage* **2024**, *87*, 111288. [CrossRef]
123. Gu, X.; Shang, Y.; Li, J.; Zhu, Y.; Tao, X.; Geng, H.; Zhang, Z.; Zhang, C. Early warning of thermal runaway based on state of safety for lithium-ion batteries. *Commun. Eng.* **2025**, *4*, 106. [CrossRef]
124. Feng, X.; Ouyang, M.; Liu, X.; Lu, L.; Xia, Y.; He, X. Thermal runaway mechanism of lithium ion battery for electric vehicles: A review. *Energy Storage Mater.* **2018**, *10*, 246–267. [CrossRef]
125. Liu, X.; Ren, D.; Hsu, H.; Feng, X.; Xu, G.-L.; Zhuang, M.; Gao, H.; Lu, L.; Han, X.; Chu, Z.; et al. Thermal Runaway of Lithium-Ion Batteries without Internal Short Circuit. *Joule* **2018**, *2*, 2047–2064. [CrossRef]
126. Christensen, P.A.; Milojevic, Z.; Wise, M.S.; Ahmeid, M.; Attidekou, P.S.; Mrozik, W.; Dickmann, N.A.; Restuccia, F.; Lambert, S.M.; Das, P.K. Thermal and mechanical abuse of electric vehicle pouch cell modules. *Appl. Therm. Eng.* **2021**, *189*, 116623. [CrossRef]
127. Encyclopedia of Electrochemical Power Sources (7-Volume Set) [2 ed.] 0323960227, 9780323960229. Available online: https://dokumen.pub/encyclopedia-of-electrochemical-power-sources-7-volume-set-2nbsped-0323960227-9780323960229.html (accessed on 8 November 2025).
128. Musso, L.; Donati, S.; Benelli, A.; Sobótka, M.; Bodak, B.; Pachnicz, M.; Fruhwirt, D.; Noone, P.; Knaup, L.; Zirker, C.; et al. Thermal runaway in lithium-ion batteries: Experimental insights from mechanical, thermal, and electrical stress tests. *Appl. Therm. Eng.* **2025**, *281*, 128661. [CrossRef]
129. Essl, C.; Golubkov, A.W.; Gasser, E.; Nachtnebel, M.; Zankel, A.; Ewert, E.; Fuchs, A. Comprehensive Hazard Analysis of Failing Automotive Lithium-Ion Batteries in Overtemperature Experiments. *Batteries* **2020**, *6*, 30. [CrossRef]
130. Das, P.K. A Perspective on the Challenges and Prospects of Realizing the Second Life of Retired EV Batteries. *Batteries* **2025**, *11*, 176. [CrossRef]
131. Ruiz, V.; Pfrang, A.; Kriston, A.; Omar, N.; Van den Bossche, P.; Boon-Brett, L. A review of international abuse testing standards and regulations for lithium ion batteries in electric and hybrid electric vehicles. *Renew. Sustain. Energy Rev.* **2018**, *81*, 1427–1452. [CrossRef]
132. Campion, C.L.; Li, W.; Lucht, B.L. Thermal Decomposition of LiPF6-Based Electrolytes for Lithium-Ion Batteries. *J. Electrochem. Soc.* **2005**, *152*, A2327. [CrossRef]
133. Jia, Z.; Qin, P.; Li, Z.; Wei, Z.; Jin, K.; Jiang, L.; Wang, Q. Analysis of gas release during the process of thermal runaway of lithium-ion batteries with three different cathode materials. *J. Energy Storage* **2022**, *50*, 104302. [CrossRef]
134. Fernandes, Y.; Bry, A.; de Persis, S. Identification and quantification of gases emitted during abuse tests by overcharge of a commercial Li-ion battery. *J. Power Sources* **2018**, *389*, 106–119. [CrossRef]
135. Ohsaki, T.; Kishi, T.; Kuboki, T.; Takami, N.; Shimura, N.; Sato, Y.; Sekino, M.; Satoh, A. Overcharge reaction of lithium-ion batteries. *J. Power Sources* **2005**, *146*, 97–100. [CrossRef]
136. Onuki, M.; Kinoshita, S.; Sakata, Y.; Yanagidate, M.; Otake, Y.; Ue, M.; Deguchi, M. Identification of the Source of Evolved Gas in Li-Ion Batteries Using C-labeled Solvents. *J. Electrochem. Soc.* **2008**, *155*, A794. [CrossRef]
137. Ribière, P.; Grugeon, S.; Morcrette, M.; Boyanov, S.; Laruelle, S.; Marlair, G. Investigation on the fire-induced hazards of Li-ion battery cells by fire calorimetry. *Energy Environ. Sci.* **2012**, *5*, 5271–5280. [CrossRef]

138. Sun, J.; Li, J.; Zhou, T.; Yang, K.; Wei, S.; Tang, N.; Dang, N.; Li, H.; Qiu, X.; Chen, L. Toxicity, a serious concern of thermal runaway from commercial Li-ion battery. *Nano Energy* **2016**, *27*, 313–319. [CrossRef]
139. Golubkov, A.W.; Scheikl, S.; Planteu, R.; Voitic, G.; Wiltsche, H.; Stangl, C.; Fauler, G.; Thaler, A.; Hacker, V. Thermal runaway of commercial 18650 Li-ion batteries with LFP and NCA cathodes—Impact of state of charge and overcharge. *RSC Adv.* **2015**, *5*, 57171–57186. [CrossRef]
140. Said, A.O.; Lee, C.; Stoliarov, S.I. Experimental investigation of cascading failure in 18650 lithium ion cell arrays: Impact of cathode chemistry. *J. Power Sources* **2020**, *446*, 227347. [CrossRef]
141. Nie, B.; Dong, Y.; Chang, L. The evolution of thermal runaway parameters of lithium-ion batteries under different abuse conditions: A review. *J. Energy Storage* **2024**, *96*, 112624. [CrossRef]
142. Milojevic, Z.; Attidekou, P.S.; Muhammad, M.; Ahmeid, M.; Lambert, S.; Das, P.K. Influence of orientation on ageing of large-size pouch lithium-ion batteries during electric vehicle life. *J. Power Sources* **2021**, *506*, 230242. [CrossRef]
143. Karp, M.; Sica, J. Evaluation of Lithium Battery Thermal Runaway Vent Gas Combustion. Available online: https://rosap.ntl.bts.gov (accessed on 8 November 2025).
144. Bouguern, M.D.; Anil Kumar, M.R.; Zaghib, K. The critical role of interfaces in advanced Li-ion battery technology: A comprehensive review. *J. Power Sources* **2024**, *623*, 235457. [CrossRef]
145. Fuhst, M.R.; Siegel, D.J. Gas Evolution in Li-Ion Batteries: Modeling Ethylene Carbonate Decomposition on $LiCoO_2$ in the Presence of Surface Magnetism. *J. Phys. Chem. C* **2020**, *124*, 24097–24104. [CrossRef]
146. Lingappan, N.; Lee, W.; Passerini, S.; Pecht, M. A comprehensive review of separator membranes in lithium-ion batteries. *Renew. Sustain. Energy Rev.* **2023**, *187*, 113726. [CrossRef]
147. Mussel-Inspired Polydopamine-Treated Polyethylene Separators for High-Power Li-Ion Batteries—Ryou—2011—Advanced Materials—Wiley Online Library. Available online: https://advanced.onlinelibrary.wiley.com/doi/abs/10.1002/adma.201100303 (accessed on 8 November 2025).
148. Thermal Stability of Lithium-Ion Batteries: A Review of Materials and Strategies. Available online: https://www.mdpi.com/1996-1073/18/16/4240 (accessed on 8 November 2025).
149. High Performance Lithium Metal Batteries Enabled by Surface Tailoring of Polypropylene Separator with a Polydopamine/Graphene Layer—Kim—2018—Advanced Energy Materials—Wiley Online Library. Available online: https://advanced.onlinelibrary.wiley.com/doi/abs/10.1002/aenm.201802665 (accessed on 8 November 2025).
150. Liu, H.; Xu, J.; Guo, B.; He, X. Effect of Al2O3/SiO2 composite ceramic layers on performance of polypropylene separator for lithium-ion batteries. *Ceram. Int.* **2014**, *40*, 14105–14110. [CrossRef]
151. Oxygen Release in Ni-Rich Layered Cathode for Lithium-Ion Batteries: Mechanisms and Mitigating Strategies—Chu—2024—ChemElectroChem—Wiley Online Library. Available online: https://chemistry-europe.onlinelibrary.wiley.com/doi/10.1002/celc.202300653 (accessed on 8 November 2025).
152. Evro, S.; Ajumobi, A.; Mayon, D.; Tomomewo, O.S. Navigating battery choices: A comparative study of lithium iron phosphate and nickel manganese cobalt battery technologies. *Future Batter.* **2024**, *4*, 100007. [CrossRef]
153. Khakani, S.E.; Rochefort, D.; MacNeil, D.D. ARC Study of LiFePO4 with Different Morphologies Prepared via Three Synthetic Routes. *J. Electrochem. Soc.* **2016**, *163*, A1311. [CrossRef]
154. Bugryniec, P.J.; Davidson, J.N.; Cumming, D.J.; Brown, S.F. Pursuing safer batteries: Thermal abuse of LiFePO4 cells. *J. Power Sources* **2019**, *414*, 557–568. [CrossRef]
155. Peng, G.; Ling, X.; Lin, Y.; Jiang, H.; Ma, M.; Yu, A.; Ouyang, D. Thermal runaway features of large-format power lithium-ion cells under various thermal abuse patterns and capacities. *RSC Adv.* **2023**, *13*, 31036–31046. [CrossRef]
156. Karmakar, A.; Zhou, H.; Vishnugopi, B.S.; Jeevarajan, J.A.; Mukherjee, P.P. State-of-Charge Implications of Thermal Runaway in Li-ion Cells and Modules. *J. Electrochem. Soc.* **2024**, *171*, 010529. [CrossRef]
157. Yi, X.; Zhang, Z.; Li, Z.; He, Y.; Liu, Q. Effect of State of Charge on Thermal Runaway Characteristics of 18650 Lithium Ion Batteries. In *Proceedings of the 2019 9th International Conference on Fire Science and Fire Protection Engineering (ICFSFPE), Chengdu, China, 18–20 October 2019*; IEEE: Piscataway, NJ, USA, 2019; pp. 1–6.
158. Kurzawski, A.; Gray, L.; Torres-Castro, L.; Hewson, J. An investigation into the effects of state of charge and heating rate on propagating thermal runaway in Li-ion batteries with experiments and simulations. *Fire Saf. J.* **2023**, *140*, 103885. [CrossRef]
159. Huang, Z.; Shen, T.; Jin, K.; Sun, J.; Wang, Q. Heating power effect on the thermal runaway characteristics of large-format lithium ion battery with $Li(Ni_{1/3}Co_{1/3}Mn_{1/3})O_2$ as cathode. *Energy* **2022**, *239*, 121885. [CrossRef]
160. Safety of Lithium-Ion Cells and Batteries at Different States-of-Charge—IOPscience. Available online: https://iopscience.iop.org/article/10.1149/1945-7111/abc8c4 (accessed on 8 November 2025).
161. Wang, B.; Zhang, F.; Zhou, X.; Wang, P.; Wang, J.; Ding, H.; Dong, H.; Liang, W.; Zhang, N.; Li, S. Which of the nickel-rich NCM and NCA is structurally superior as a cathode material for lithium-ion batteries? *J. Mater. Chem. A* **2021**, *9*, 13540–13551. [CrossRef]

162. Quantitative Evaluation of Thermal Runaway in Lithium-Ion Batteries Under Critical Heating Conditions to Enhance Safety | Scientific Reports. Available online: https://www.nature.com/articles/s41598-025-07824-7 (accessed on 8 November 2025).
163. Huang, Z.; Liu, J.; Zhai, H.; Wang, Q. Experimental investigation on the characteristics of thermal runaway and its propagation of large-format lithium ion batteries under overcharging and overheating conditions. *Energy* **2021**, *233*, 121103. [CrossRef]
164. Zhang, X.; Zhang, H.; Almansour, A.; Singh, M.; Kiser, J.D.; Zhu, H.; Halbig, M.C.; Zheng, Y. A Comprehensive Analysis of Thermal Heat Dissipation for Lithium-Ion Battery Packs. *Energies* **2025**, *18*, 2234. [CrossRef]
165. Song, L.; Zhou, Z.; Ju, X.; Wang, B.; Rojas-Alva, U.; Zhou, X.; Yang, L. Experimental study on thermal runaway characteristics and fire hazards of lithium-ion batteries in semi-confined space of transportation. *J. Energy Storage* **2025**, *128*, 117220. [CrossRef]
166. In-Operando High-Speed Tomography of Lithium-Ion Batteries During Thermal Runaway | Nature Communications. Available online: https://www.nature.com/articles/ncomms7924 (accessed on 8 November 2025).
167. Shasqil. The Hidden Threat of Jet Fire and an Unlikely Solution. Available online: https://ancloz.com/the-hidden-threat-of-jet-fire-and-an-unlikely-solution-removable-pfp-jacket/ (accessed on 31 July 2025).
168. HSE Offshore: Fire and Explosion Strategy—Jet Fires. Available online: https://www.hse.gov.uk/offshore/strategy/jet.htm (accessed on 31 July 2025).
169. Ada. Signs of Cutaneous Burns. Available online: https://ada.com/conditions/cutaneous-burns/ (accessed on 31 July 2025).
170. "Unconscious after two breaths": Lithium battery explosions in South Korea killed 22 through smoke inhalation | CTIF—International Association of Fire Services for Safer Citizens through Skilled Firefighters. Available online: https://ctif.org/news/unconscious-after-two-breaths-lithium-battery-explosions-south-korea-killed-22-through-smoke (accessed on 31 July 2025).
171. Carbon dioxide—IDLH | NIOSH | CDC. Available online: https://www.cdc.gov/niosh/idlh/124389.html (accessed on 23 August 2025).
172. Table of IDLH Values | NIOSH | CDC. Available online: https://www.cdc.gov/niosh/idlh/intridl4.html (accessed on 25 August 2025).
173. Carbon Dioxide | Wisconsin Department of Health Services. Available online: https://www.dhs.wisconsin.gov/chemical/carbondioxide.htm (accessed on 26 August 2025).
174. NASA Global Climate Change. Carbon Dioxide Concentration | NASA Global Climate Change. Available online: https://climate.nasa.gov/vital-signs/carbon-dioxide?intent=121 (accessed on 26 August 2025).
175. Carbon Monoxide—IDLH | NIOSH | CDC. Available online: https://www.cdc.gov/niosh/idlh/630080.html (accessed on 23 August 2025).
176. Carbon Monoxide & Health | California Air Resources Board. Available online: https://ww2.arb.ca.gov/resources/carbon-monoxide-and-health (accessed on 26 August 2025).
177. Alternative Fuels Data Center: Hydrogen Benefits and Considerations. Available online: https://afdc.energy.gov/fuels/hydrogen-benefits (accessed on 2 September 2025).
178. Steamy Relationships: How Atmospheric Water Vapor Amplifies Earth's Greenhouse Effect—NASA Science. Available online: https://science.nasa.gov/earth/climate-change/steamy-relationships-how-atmospheric-water-vapor-amplifies-earths-greenhouse-effect/ (accessed on 2 September 2025).
179. U.S. Environmental Protection Agency. Importance of Methane. Available online: https://www.epa.gov/gmi/importance-methane (accessed on 2 September 2025).
180. Canadian Centre for Occupational Health and Safety; Government of Canada. CCOHS: Methane. Available online: https://www.ccohs.ca/oshanswers/chemicals/chem_profiles/methane.html (accessed on 2 September 2025).
181. Health Canada. Ethene Public Summary. Available online: https://www.canada.ca/en/health-canada/services/chemical-substances/fact-sheets/chemicals-glance/ethene-pubic-summary.html (accessed on 2 September 2025).
182. Environment and Climate Change Canada (ECCC). Screening assessment report ethane propane isobutane butane butane (branched and linear). Available online: https://www.canada.ca/en/environment-climate-change/services/evaluating-existing-substances/screening-assessment-ethane-propane-isobutane-butane.html (accessed on 2 September 2025).
183. Canadian Centre for Occupational Health and Safety; Government of Canada. CCOHS: Propane. Available online: https://www.ccohs.ca/oshanswers/chemicals/chem_profiles/propane.html (accessed on 26 August 2025).
184. Alternative Fuels Data Center: Propane Vehicle Emissions. Available online: https://afdc.energy.gov/vehicles/propane-emissions (accessed on 26 August 2025).
185. PubChem Propylene. Available online: https://pubchem.ncbi.nlm.nih.gov/compound/Propylene (accessed on 2 September 2025).
186. Health Canada. Propene (1-Propene). Available online: https://www.canada.ca/en/health-canada/services/chemical-substances/fact-sheets/chemicals-glance/propene.html (accessed on 2 September 2025).
187. CDC Hydrogen Fluoride. Available online: https://www.cdc.gov/chemical-emergencies/chemical-fact-sheets/hydrogen-fluoride.html (accessed on 2 September 2025).
188. Hydrogen Fluoride/Hydrofluoric Acid: Systemic Agent | NIOSH | CDC. Available online: https://www.cdc.gov/niosh/ershdb/emergencyresponsecard_29750030.html (accessed on 2 September 2025).

189. PubChem Trifluoromethane. Available online: https://pubchem.ncbi.nlm.nih.gov/compound/6373 (accessed on 3 September 2025).
190. What are the Impacts of PFAS Polymers on Our Health and the Environment? Available online: https://www.eea.europa.eu/en/newsroom/news/impacts-of-pfas-polymers (accessed on 3 September 2025).
191. U.S. Environmental Protection Agency. Sulfur Dioxide Basics. Available online: https://www.epa.gov/so2-pollution/sulfur-dioxide-basics (accessed on 3 September 2025).
192. Sulfur Dioxide—IDLH | NIOSH | CDC. Available online: https://www.cdc.gov/niosh/idlh/7446095.html (accessed on 3 September 2025).
193. Acrolein—IDLH | NIOSH | CDC. Available online: https://www.cdc.gov/niosh/idlh/107028.html (accessed on 3 September 2025).
194. National Research Council; Division On Earth And Life Studies; Board On Environmental Studies And Toxic. Acrolein Acute Exposure Guideline Levels. In *Acute Exposure Guideline Levels for Selected Airborne Chemicals: Volume 8*; National Academies Press: Bethesda, MD, USA, 2010.
195. Canada, H. Residential indoor air quality guidelines: Acrolein. Available online: https://www.canada.ca/en/health-canada/services/publications/healthy-living/residential-indoor-air-quality-guidelines-acrolein.html (accessed on 3 September 2025).
196. Bein, K.; Leikauf, G.D. Acrolein—A pulmonary hazard. *Mol. Nutr. Food Res.* **2011**, *55*, 1342–1360. [CrossRef] [PubMed]
197. CDC Benzene. Available online: https://www.cdc.gov/chemical-emergencies/chemical-fact-sheets/benzene.html (accessed on 25 August 2025).
198. Benzene—DCCEEW. Available online: https://www.dcceew.gov.au/environment/protection/npi/resource/student/benzene (accessed on 26 August 2025).
199. CDC—NIOSH Pocket Guide to Chemical Hazards—Diphenyl. Available online: https://www.cdc.gov/niosh/npg/npgd0239.html (accessed on 2 September 2025).
200. PubChem Biphenyl. Available online: https://pubchem.ncbi.nlm.nih.gov/compound/Biphenyl (accessed on 2 September 2025).
201. Health Effects. In *Toxicological Profile for Toluene*; Agency for Toxic Substances and Disease Registry: Atlanta, GA, USA, 2017. Available online: https://www.ncbi.nlm.nih.gov/books/NBK592498/ (accessed on 2 September 2025).
202. Toluene (Methylbenzene)—DCCEEW. Available online: https://www.dcceew.gov.au/environment/protection/npi/substances/fact-sheets/toluene-methylbenzene (accessed on 2 September 2025).
203. PubChem. Styrene. Available online: https://pubchem.ncbi.nlm.nih.gov/compound/7501 (accessed on 2 September 2025).

Disclaimer/Publisher's Note: The statements, opinions and data contained in all publications are solely those of the individual author(s) and contributor(s) and not of MDPI and/or the editor(s). MDPI and/or the editor(s) disclaim responsibility for any injury to people or property resulting from any ideas, methods, instructions or products referred to in the content.